nature genetics

BMP signaling controls muscle mass

Roberta Sartori[1,2,11], Elija Schirwis[3–5,11], Bert Blaauw[2], Sergia Bortolanza[1,2], Jinghui Zhao[6], Elena Enzo[2], Amalia Stantzou[3,4], Etienne Mouisel[3], Luana Toniolo[2], Arnaud Ferry[3], Sigmar Stricker[7], Alfred L Goldberg[6], Sirio Dupont[2], Stefano Piccolo[2], Helge Amthor[3,4,8] & Marco Sandri[1,2,9,10]

Cell size is determined by the balance between protein synthesis and degradation. This equilibrium is affected by hormones, nutrients, energy levels, mechanical stress and cytokines. Mutations that inactivate myostatin lead to excessive muscle growth in animals and humans, but the signals and pathways responsible for this hypertrophy remain largely unknown. Here we show that bone morphogenetic protein (BMP) signaling, acting through Smad1, Smad5 and Smad8 (Smad1/5/8), is the fundamental hypertrophic signal in mice. Inhibition of BMP signaling causes muscle atrophy, abolishes the hypertrophic phenotype of myostatin-deficient mice and strongly exacerbates the effects of denervation and fasting. BMP-Smad1/5/8 signaling negatively regulates a gene (*Fbxo30*) that encodes a ubiquitin ligase required for muscle loss, which we named muscle ubiquitin ligase of the SCF complex in atrophy-1 (MUSA1). Collectively, these data identify a critical role for the BMP pathway in adult muscle maintenance, growth and atrophy.

Skeletal muscle is a major site of metabolic activity and is the most abundant tissue in the human body. During development, the growth of skeletal muscle mass depends on protein and cellular turnover[1]. In adulthood, skeletal muscle adapts its size and function to different physiological requirements and pathophysiological conditions, primarily by affecting pathways regulating protein turnover. In particular, the size of post-mitotic cells is determined by a balance between new protein accumulation and the degradation of existing proteins[2]. Few pathways have been identified that regulate muscle growth in adulthood, and, among these, myostatin—a transforming growth factor (TGF)-β family member—has a key role as a negative regulator[3,4]. Myostatin signals via the activin type II receptors (ActRIIA and ActRIIB) and activin type I receptors (ALK4 and ALK5) to phosphorylate responsive Smad proteins (Smad2 and Smad3, Smad2/3), which enables the Smad proteins to form a transcriptional complex with Smad4 to transcribe target genes. Several genetic and biochemical studies have shown that inhibition of the myostatin-ActRIIB-ALK4/ALK5-Smad2/3 pathway promotes muscle hypertrophy in adulthood[5,6]. However, the target genes and mechanisms that drive muscle hypertrophy downstream of myostatin inhibition remain unclear.

BMPs are cytokines of the TGF-β superfamily that bind to dedicated BMP receptors (for example, ALK3) that in turn phosphorylate BMP-responsive Smad proteins (Smad1/5/8)[7]. Similar to Smad2 and Smad3, BMP-dependent Smad proteins also form a transcriptional complex with Smad4 that translocates to the nucleus and regulates the transcription of target genes, including the inhibitor of DNA binding (ID) gene family. ID proteins (ID1, ID2, ID3 and ID4) belong to the E-protein family and control cell growth and differentiation[8]. BMP signaling is mostly known for its roles in embryonic development and in bone/cartilage formation[7]. In adult skeletal muscle, activation of BMPs has been associated with ectopic bone and cartilage formation and with diseases such as fibrodysplasia ossificans progressiva[9]. The role of endogenous BMP signaling in the homeostasis of adult tissues and its relationship with myostatin signaling remain largely unknown.

RESULTS

Generation of muscle-specific *Smad4* knockout mice

To explore the relationship between myostatin and BMP signaling, we generated muscle-specific *Smad4* knockout mice (**Supplementary Fig. 1**). PCR, immunoblot and immunohistochemistry analyses confirmed the absence of Smad4 in the muscles of *Smad4*$^{-/-}$ mice (**Supplementary Fig. 1a–e**). Functional inhibition of Smad4 in skeletal muscle was confirmed by suppression of the CAGA12 luciferase reporter (a Smad3 sensor[10]) and the *Id1-BRE* luciferase reporter (a Smad1/5/8 sensor[11]) (**Supplementary Fig. 1f,g**). Altogether, these findings validate our genetic mouse model of inhibition of the BMP and myostatin pathways.

[1]Dulbecco Telethon Institute at the Venetian Institute of Molecular Medicine, Padova, Italy. [2]Department of Biomedical Sciences, University of Padova, Padova, Italy. [3]Université Pierre et Marie Curie, Institut de Myologie, UMR Université Pierre et Marie Curie–Association Institut de Myologie (AIM), Unité Mixte 76, INSERM U974, CNRS UMR 7215, Paris, France. [4]UFR (Unité de Formation et de Recherche) des Sciences de la Santé, Université de Versailles Saint-Quentin-en-Yvelines, Montigny-le-Bretonneux, France. [5]Entwicklungsbiologie/Signaltransduktion, Max Delbrück Center for Molecular Medicine, Berlin, Germany. [6]Department of Cell Biology, Harvard Medical School, Boston, Massachusetts, USA. [7]Development and Disease Group, Max Planck Institute for Molecular Genetics, Berlin, Germany. [8]Service Génétique Médicale, Centre Hospitalier Universitaire Necker–Enfants Malades, Université Paris Descartes, Paris, France. [9]Institute of Neuroscience, Consiglio Nazionale delle Ricerche, Padova, Italy. [10]Department of Medicine, McGill University, Montreal, Quebec, Canada. [11]These authors contributed equally to this work. Correspondence should be addressed to M.S. (marco.sandri@unipd.it), H.A. (helge.amthor@uvsq.fr) or S.P. (stefano.piccolo@unipd.it).

Received 23 January; accepted 3 September; published online 29 September 2013; doi:10.1038/ng.2772

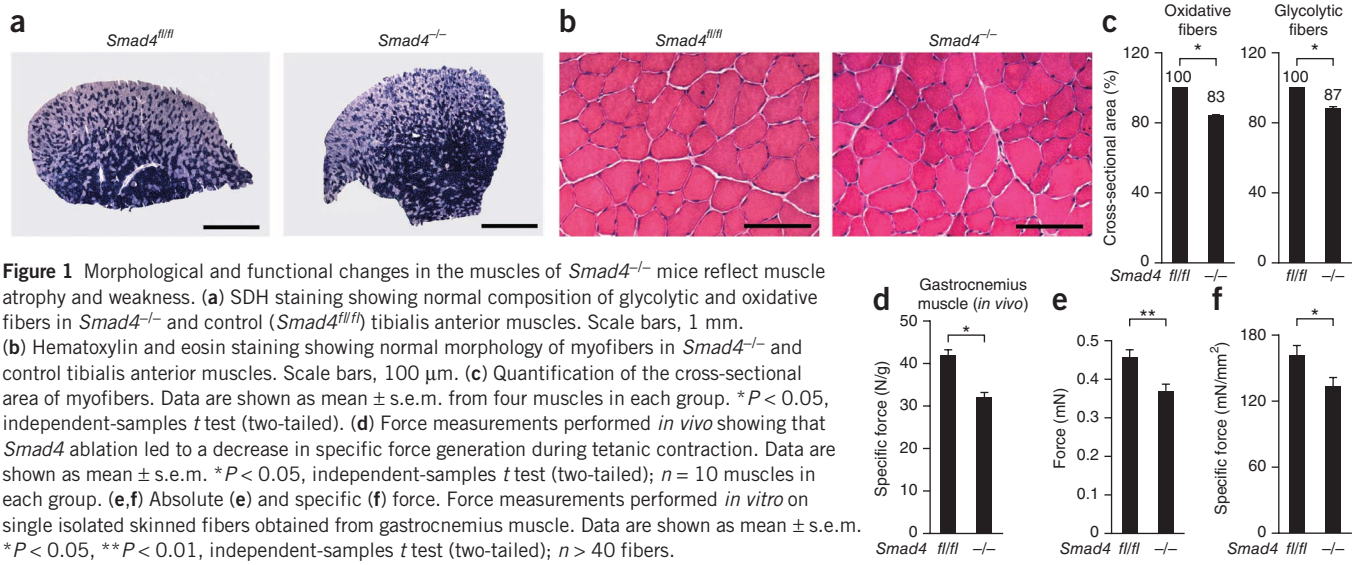

Figure 1 Morphological and functional changes in the muscles of *Smad4*$^{-/-}$ mice reflect muscle atrophy and weakness. (**a**) SDH staining showing normal composition of glycolytic and oxidative fibers in *Smad4*$^{-/-}$ and control (*Smad4*$^{fl/fl}$) tibialis anterior muscles. Scale bars, 1 mm. (**b**) Hematoxylin and eosin staining showing normal morphology of myofibers in *Smad4*$^{-/-}$ and control tibialis anterior muscles. Scale bars, 100 μm. (**c**) Quantification of the cross-sectional area of myofibers. Data are shown as mean ± s.e.m. from four muscles in each group. *$P < 0.05$, independent-samples *t* test (two-tailed). (**d**) Force measurements performed *in vivo* showing that *Smad4* ablation led to a decrease in specific force generation during tetanic contraction. Data are shown as mean ± s.e.m. *$P < 0.05$, independent-samples *t* test (two-tailed); $n = 10$ muscles in each group. (**e**,**f**) Absolute (**e**) and specific (**f**) force. Force measurements performed *in vitro* on single isolated skinned fibers obtained from gastrocnemius muscle. Data are shown as mean ± s.e.m. *$P < 0.05$, **$P < 0.01$, independent-samples *t* test (two-tailed); $n > 40$ fibers.

Smad4 deficiency induces muscle atrophy and weakness

The resulting *Smad4*$^{-/-}$ mice were indistinguishable in appearance from mice with *lox*P-flanked *Smad4* alleles (*Smad4*$^{fl/fl}$ mice). Staining for succinate dehydrogenase (SDH) showed no major alteration in the distribution of β-oxidative versus glycolytic fibers (**Fig. 1**). Histological analysis of adult muscle showed normal muscle architecture and absence of myopathic features in knockout mice. However, quantification of cross-sectional area showed a slight but significant decrease in myofiber size, both in glycolytic and oxidative fibers of different muscles (**Fig. 1c** and **Supplementary Fig. 2a–c**). To understand whether the reduction in myofiber size affects muscle performance, we measured the strength of the gastrocnemius muscle in living mice. Maximal absolute force (tetanic force) was slightly reduced (**Fig. 2**), whereas specific force was significantly lower in

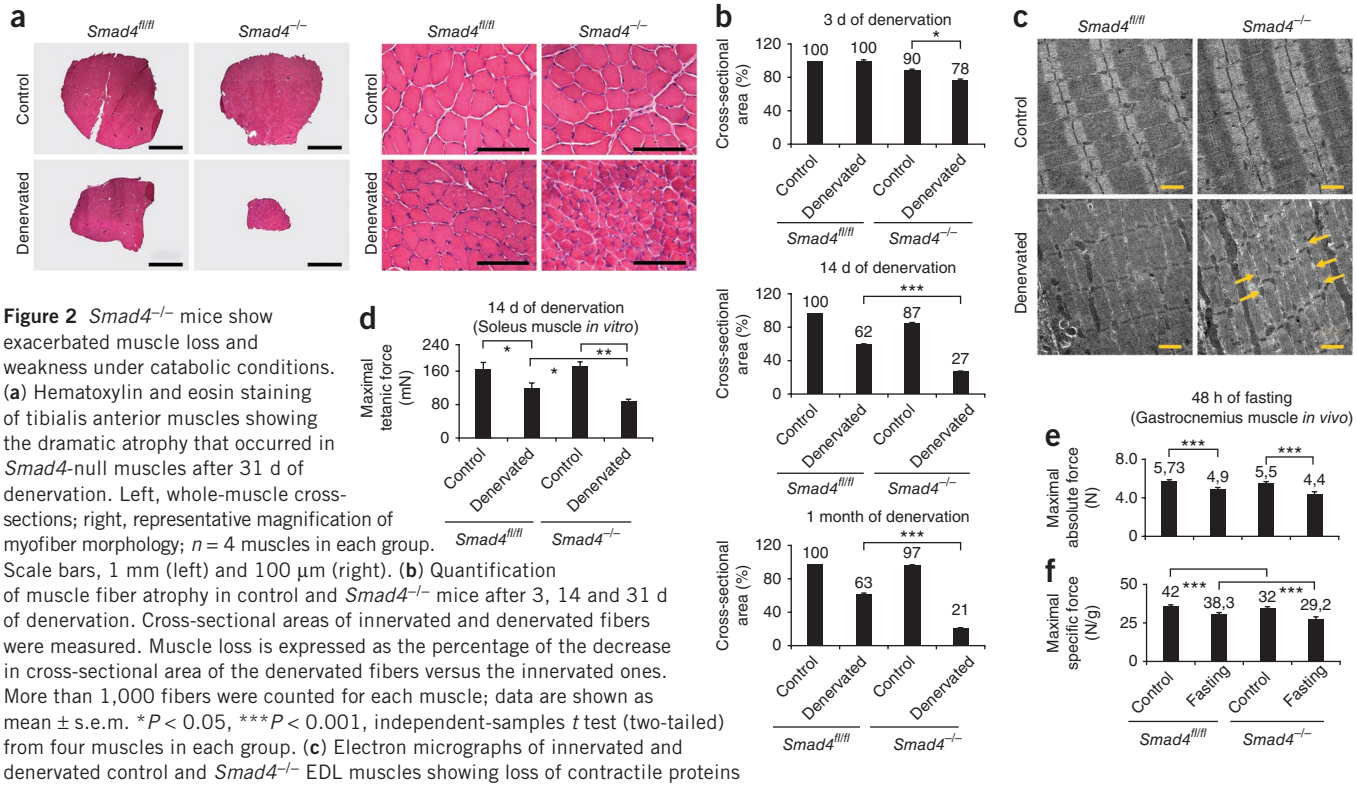

Figure 2 *Smad4*$^{-/-}$ mice show exacerbated muscle loss and weakness under catabolic conditions. (**a**) Hematoxylin and eosin staining of tibialis anterior muscles showing the dramatic atrophy that occurred in *Smad4*-null muscles after 31 d of denervation. Left, whole-muscle cross-sections; right, representative magnification of myofiber morphology; $n = 4$ muscles in each group. Scale bars, 1 mm (left) and 100 μm (right). (**b**) Quantification of muscle fiber atrophy in control and *Smad4*$^{-/-}$ mice after 3, 14 and 31 d of denervation. Cross-sectional areas of innervated and denervated fibers were measured. Muscle loss is expressed as the percentage of the decrease in cross-sectional area of the denervated fibers versus the innervated ones. More than 1,000 fibers were counted for each muscle; data are shown as mean ± s.e.m. *$P < 0.05$, ***$P < 0.001$, independent-samples *t* test (two-tailed) from four muscles in each group. (**c**) Electron micrographs of innervated and denervated control and *Smad4*$^{-/-}$ EDL muscles showing loss of contractile proteins that resulted in thinner myofibrils (arrows). Scale bars, 1 μm. (**d**) Force measurements performed *ex vivo* on soleus muscle showed that absence of *Smad4* led to a profound decrease in the maximal force generated during tetanic contraction in denervated muscles compared to in control muscle. Data are shown as mean ± s.e.m. *$P < 0.05$, **$P < 0.01$, independent-samples *t* test (two-tailed); $n = 8$ muscles in each group. (**e**,**f**) Force measurements performed *in vivo* on gastrocnemius muscle. Absence of *Smad4* led to a significant decrease in the maximal absolute force (**e**) but not in the maximal specific force (**f**) generated during tetanic contraction after fasting that was greater in *Smad4*$^{-/-}$ than in control mice. Data are shown as mean ± s.e.m. ***$P < 0.001$, independent-samples *t* test (two-tailed); $n = 10$ muscles in each group.

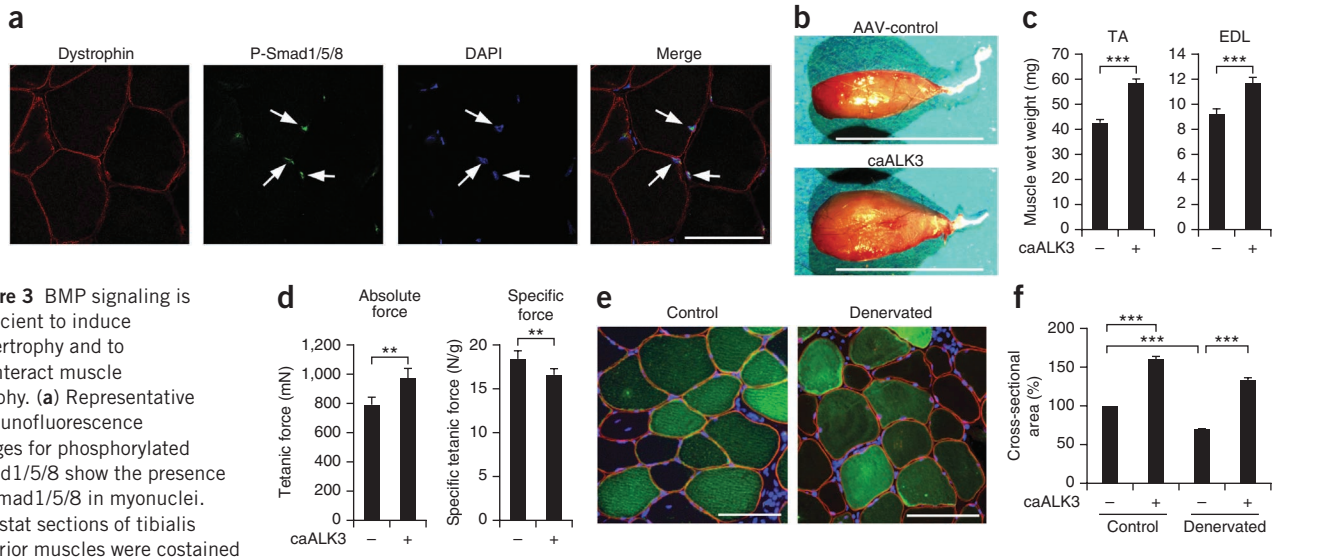

Figure 3 BMP signaling is sufficient to induce hypertrophy and to counteract muscle atrophy. (**a**) Representative immunofluorescence images for phosphorylated Smad1/5/8 show the presence of Smad1/5/8 in myonuclei. Cryostat sections of tibialis anterior muscles were costained for dystrophin (red), phosphorylated Smad1/5/8 (P-Smad1/5/8; green) and DAPI (blue). Note the presence of phosphorylated Smad1/5/8 in myonuclei, which can be identified by their subsarcolemmal localization, as indicated in the merged image (arrows); $n = 4$ wild-type muscles. Scale bar, 50 µm. (**b**) Activation of the BMP pathway stimulates muscle growth. Adult tibialis anterior and EDL muscles were transfected with AAV encoding caALK3 (AAV-caALK3) or encoding a non-functional construct, U7-c (AAV-control) and were examined 7 weeks later. Representative tibialis anterior muscles are depicted; $n = 5$ for each condition. Scale bars, 1 cm. (**c**) The weight of transfected muscles was measured; data are shown as mean ± s.e.m. $^{***}P < 0.001$, paired-samples *t* test (two-tailed); $n = 5$ muscles for each condition. TA, tibialis anterior. (**d**) Force measurements of transfected tibialis anterior muscles performed *in vivo* showing that overexpression of caALK3 leads to a significant increase in maximal absolute force but not in specific force, which is slightly reduced. Data are shown as mean ± s.e.m. $^{**}P < 0.01$, paired-samples *t* test (two-tailed); $n = 5$ for each condition. (**e**) Activation of the BMP pathway protects from muscle atrophy. Adult muscle fibers were cotransfected with constructs expressing caALK3 and EGFP, denervated and examined 12 d later. Green, EGFP; red, dystrophin staining; blue, Hoechst staining of myonuclei. Scale bars, 70 µm. (**f**) Cross-sectional areas of transfected fibers, identified by EGFP fluorescence, were measured. Data are shown as mean ± s.e.m. $^{***}P < 0.001$, independent-samples *t* test (two-tailed); $n = 4$ muscles for each condition.

Smad4$^{-/-}$ mice (**Fig. 1d**). To explain this decrease in specific force, we quantified myofiber number in gastrocnemius muscles from control and knockout mice. Hyperplasia was present in *Smad4*$^{-/-}$ gastrocnemius muscle, causing an increase in muscle weight (**Supplementary Fig. 2d**,**e**). To evaluate force production at the single-fiber level, we recorded muscle force on isolated single skinned fibers obtained from gastrocnemius muscle. This approach allowed us to explore the force generated by sarcomeric proteins independent of fiber number, innervation, ATP levels and calcium release. Both absolute and specific forces were significantly reduced in *Smad4*-deficient mice (**Fig. 1e**,**f**). Thus, hyperplasia compensates for atrophy and weakness in *Smad4*$^{-/-}$ mice.

To further understand the role of Smad4 in muscle, we analyzed the phenotype of *Smad4*$^{-/-}$ mice under conditions of muscle wasting. We used two models of muscle atrophy—denervation and fasting. Surprisingly, *Smad4*$^{-/-}$ mice lost significantly more muscle mass after denervation than *Smad4*$^{fl/fl}$ control mice (**Fig. 2a**,**b**). Quantification of cross-sectional area showed 38% and 73% decreases in control and *Smad4*$^{-/-}$ muscles, respectively, 14 d after denervation (**Fig. 2b**). After 1 month of denervation, *Smad4*-deficient muscles were almost completely absent (**Fig. 2a**,**b** and **Supplementary Fig. 3a–c**). Electron microscopy showed no major structural abnormalities but confirmed the presence of excessive proteolysis in denervated *Smad4*$^{-/-}$ muscle (**Fig. 2c** and **Supplementary Fig. 4**). Furthermore, absolute muscle force, an index of contractile protein breakdown, was significantly weaker in *Smad4*$^{-/-}$ soleus muscle than in *Smad4*$^{fl/fl}$ soleus muscle after denervation (**Fig. 2d** and **Supplementary Fig. 5a**,**b**).

We next monitored the relevance of *Smad4* deficiency during fasting[12,13]. Functional measurements of gastrocnemius muscle strength *in vivo* confirmed that the loss of maximal absolute force after fasting was greater in *Smad4*$^{-/-}$ mice than in controls (**Fig. 2e** and **Supplementary Fig. 5c**), indicating greater loss of sarcomeric proteins. This conclusion is supported by the fact that the specific force (force normalized by muscle mass) was not significantly affected by fasting in wild-type or knockout mice (**Fig. 2f** and **Supplementary Fig. 5d**,**e**).

Activation of BMPs induces muscle growth and blocks atrophy

The data presented above indicate that Smad4, a shared element of the myostatin and BMP pathways, is required to maintain muscle mass and prevent muscle wasting. Immunohistochemistry confirmed the presence of phosphorylated Smad1/5/8 in the nuclei of myofibers (**Fig. 3a**), suggesting that the BMP pathway is normally active in adult muscles. We then asked whether activation of BMP signaling promotes muscle hypertrophy. To explore this hypothesis, we tested the ability of a constitutively active type I BMP receptor (caALK3) to affect muscle mass. Adeno-associated virus (AAV)-mediated overexpression of caALK3 increased the phosphorylation of Smad1/5/8, the downstream transcription factors, whereas it did not affect expression of components of the TGF-β and BMP pathways (**Supplementary Fig. 6**). Notably, caALK3 was sufficient to trigger massive muscle hypertrophy in adult tibialis anterior muscle (**Fig. 3b** and **Supplementary Fig. 6d**,**e**). AAV-mediated caALK3 expression also triggered fiber instability, followed by degeneration and regeneration, which likely resulted from the massive and fast hypertrophy (**Supplementary Fig. 6d–f**). Activated ALK3 promoted 35% and 20% increases in the mass of tibialis anterior and extensor digitorum longus (EDL) muscles, respectively (**Fig. 3c**), consistent with increases in fiber size (**Supplementary Fig. 6e**) and maximal force (**Fig. 3d**). The presence of degenerating and regenerating

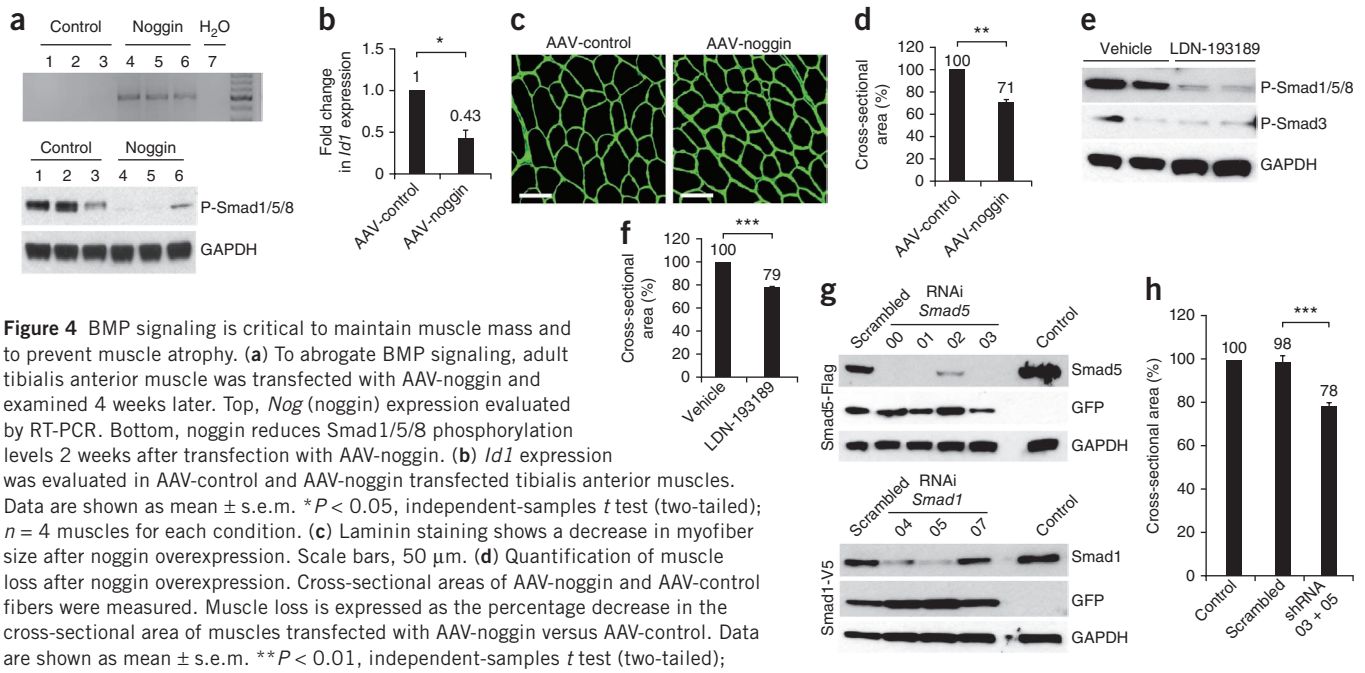

Figure 4 BMP signaling is critical to maintain muscle mass and to prevent muscle atrophy. (**a**) To abrogate BMP signaling, adult tibialis anterior muscle was transfected with AAV-noggin and examined 4 weeks later. Top, *Nog* (noggin) expression evaluated by RT-PCR. Bottom, noggin reduces Smad1/5/8 phosphorylation levels 2 weeks after transfection with AAV-noggin. (**b**) *Id1* expression was evaluated in AAV-control and AAV-noggin transfected tibialis anterior muscles. Data are shown as mean ± s.e.m. $^{*}P < 0.05$, independent-samples *t* test (two-tailed); $n = 4$ muscles for each condition. (**c**) Laminin staining shows a decrease in myofiber size after noggin overexpression. Scale bars, 50 μm. (**d**) Quantification of muscle loss after noggin overexpression. Cross-sectional areas of AAV-noggin and AAV-control fibers were measured. Muscle loss is expressed as the percentage decrease in the cross-sectional area of muscles transfected with AAV-noggin versus AAV-control. Data are shown as mean ± s.e.m. $^{**}P < 0.01$, independent-samples *t* test (two-tailed); myofibers of the entire muscle cross-section were analyzed, $n = 4$ muscles for each condition. (**e**,**f**) LDN-193189 treatment reduces phosphorylation of Smad1/5/8 but not of Smad3 (P-Smad3) (**e**) and causes muscle atrophy (**f**). LDN-193189 was injected intraperitoneally twice per day for 9 d at the dose of 3 mg/kg. Data are shown as mean ± s.e.m. $^{***}P < 0.001$, independent-samples *t* test (two-tailed); $n = 2{,}500$ fibers for each condition; $n = 4$ muscles in each group. (**g**) RNA interference (RNAi)-mediated knockdown of Smad1 and Smad5 shown by immunoblotting. Mouse embryonic fibroblasts (MEFs) were transfected with vectors expressing different shRNAs against *Smad5* (top) and *Smad1* (bottom) together with vectors encoding mouse Smad1-V5 and Smad5-Flag, respectively. Cells expressing Smad5-V5 or Smad1-Flag but not shRNAs were set as control. (**h**) Combined inhibition of Smad1 and Smad5 causes muscle fiber atrophy. Adult muscle fibers were cotransfected with bicistronic expression vectors that encode shRNAs specific for either *Smad1* or *Smad5* and EGFP. Two weeks later, cross-sectional areas of transfected fibers, identified by GFP fluorescence, were measured. Data are shown as mean ± s.e.m. $^{***}P < 0.001$, independent-samples *t* test (two-tailed); $n = 8$ muscles for each group.

fibers explained the slight decrease in specific force (**Fig. 3d** and **Supplementary Fig. 6f**). ALK3-mediated hypertrophy was completely prevented by pharmacological inhibition of BMP type I receptor and by *Smad4* deletion (**Supplementary Fig. 7a**,**b**). Next, we determined whether ALK3 activity could prevent muscle loss after denervation. We expressed caALK3 in denervated muscles through electroporation and quantified myofiber size after 12 d. Activation of the BMP pathway induced hypertrophy of innervated muscle fibers, confirming the effect of AAV-mediated overexpression of caALK3 (**Fig. 3e**,**f**). Notably, caALK3 not only prevented muscle atrophy but also induced hypertrophy of denervated fibers (**Fig. 3e**,**f**). These growth-promoting effects of caALK3 were completely blunted in $Smad4^{-/-}$ mice (**Supplementary Fig. 7c**).

Inhibition of the BMP pathway leads to muscle atrophy

We then asked whether inhibition of BMP signaling induces muscle atrophy. BMPs are antagonized by noggin, a secreted protein that blocks the binding of BMPs to their receptors[14,15]. Overexpression of noggin (**Fig. 4a**, top and **Supplementary Fig. 8**) in adult tibialis anterior muscles reduced expression of *Id1* (**Fig. 4b**), abolished phosphorylation of Smad1/5/8 (**Fig. 4a**, bottom) and induced atrophy (**Fig. 4c**,**d**). Notably, overexpression of noggin did not trigger compensatory feedback loops for the TGF-β and BMP pathways (**Fig. 4a** and **Supplementary Fig. 8b**,**c**). Next, we treated wild-type mice for 9 d with LDN-193189, an inhibitor of BMP type I receptors[9], which decreased basal phosphorylation of Smad1/5/8 and caused 21% atrophy of tibialis anterior myofibers (**Fig. 4e**,**f**). Notably, LDN-193189 treatment did not affect the phosphorylation of Smad3 (**Fig. 4e** and **Supplementary Fig. 9**). To prove the role of Smad1/5/8 in controlling muscle mass, we knocked down *Smad1* or *Smad5* in adult muscles *in vivo*. We tested seven different short hairpin RNAs (shRNAs) for their ability to reduce Smad5 or Smad1 protein levels. Three of these efficiently knocked down Smad5, whereas two reduced Smad1 protein levels (**Fig. 4g**). Moreover, all these oligonucleotides blocked ALK3-mediated activation of an *Id1* reporter (**Supplementary Fig. 10a**,**b**), with oligo 03 against *Smad5* and oligo 05 against *Smad1* being the most efficient at blocking induction of the Smad1/5/8 sensor in the presence of caALK3. When oligos 03 and 05 were cotransfected into tibialis anterior muscle *in vivo*, they efficiently reduced the levels of phosphorylated Smad1/5/8 (**Supplementary Fig. 10c**). After 2 weeks of shRNA-mediated *Smad1* and *Smad5* knockdown, myofiber size was reduced by 20% (**Fig. 4h**).

It is worth noting that *Smad4* deletion caused the strongest effect under denervation or fasting. Thus, it is possible that denervation activates BMPs as a means to counteract muscle wasting. Notably, denervation induced the *ID1* reporter, both at 6 and 12 d after neurectomy, confirming that the BMP pathway is activated in atrophying muscles (**Fig. 5a**). Consistently, Smad1/5/8 phosphorylation mirrored *ID1* reporter activity, being higher in denervated than in innervated muscles (**Fig. 5b**). We then studied the expression of BMP and myostatin genes in control and denervated muscles. Interestingly, whereas several BMP genes were expressed in innervated muscles, only *Gdf6* (encoding BMP13) and *Gdf5* (encoding BMP14) were strongly induced after denervation (**Fig. 5c**). Moreover, the expression of BMP receptors was induced during atrophy, whereas expression of *Mstn* (encoding myostatin) and *Acvr2b* (encoding ActRIIB) was downregulated (**Fig. 5c** and **Supplementary Fig. 11**).

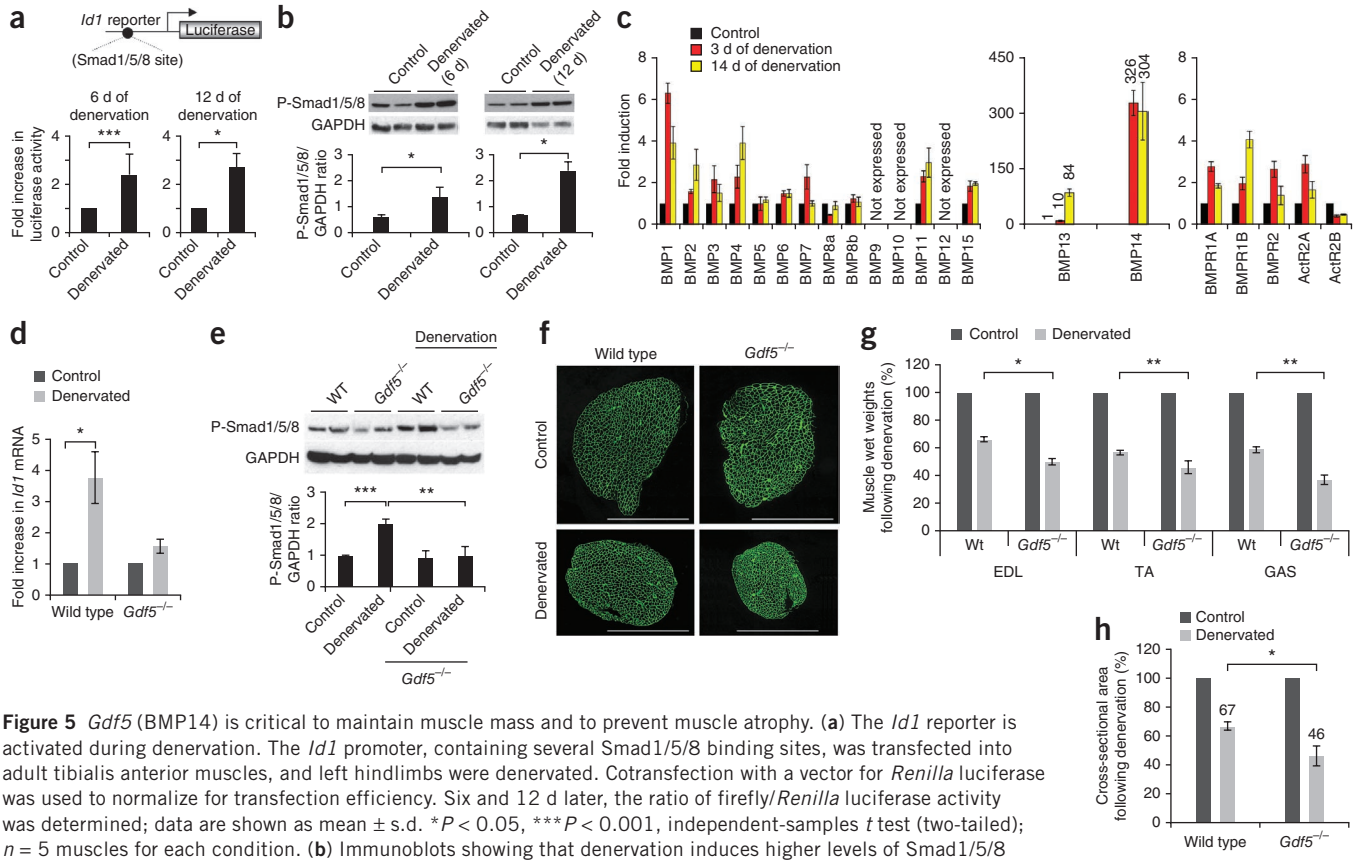

Figure 5 *Gdf5* (BMP14) is critical to maintain muscle mass and to prevent muscle atrophy. (**a**) The *Id1* reporter is activated during denervation. The *Id1* promoter, containing several Smad1/5/8 binding sites, was transfected into adult tibialis anterior muscles, and left hindlimbs were denervated. Cotransfection with a vector for *Renilla* luciferase was used to normalize for transfection efficiency. Six and 12 d later, the ratio of firefly/*Renilla* luciferase activity was determined; data are shown as mean ± s.d. $*P < 0.05$, $***P < 0.001$, independent-samples *t* test (two-tailed); $n = 5$ muscles for each condition. (**b**) Immunoblots showing that denervation induces higher levels of Smad1/5/8 phosphorylation 6 and 12 d after neurectomy. Data are shown as mean ± s.e.m. $*P < 0.05$, independent-samples *t* test (two-tailed); $n = 4$ muscles for each condition. (**c**) Transcript expression levels of different BMPs and their receptors in innervated and denervated tibialis anterior muscles. Data are shown as mean ± s.e.m.; $n = 4$ muscles for each condition. (**d**) *Id1* expression was evaluated in innervated and denervated muscles from wild-type and *Gdf5*-mutant mice; data are shown as mean ± s.e.m. $*P < 0.05$, paired-samples *t* test (two-tailed); $n = 4$ for each condition. (**e**) Immunoblot showing that denervation induces phosphorylation of Smad1/5/8 in wild-type (WT) but not in *Gdf5*-mutant mice. Data are shown as mean ± s.e.m. $***P < 0.001$, $**P < 0.01$, paired-samples *t* test (two-tailed); $n = 6$ muscles for each condition. (**f**) Laminin staining of innervated and denervated EDL muscles from wild-type and *Gdf5*-mutant mice. Absence of *Gdf5* leads to stronger muscle atrophy. Mosaic images were acquired using automated scanning with a 20× objective. Scale bar, 1 mm. (**g**) Quantification of muscle loss in the EDL, tibialis anterior and gastrocnemius (GAS) muscles of denervated wild-type and *Gdf5*-mutant mice. Data show muscle weight expressed as percentage of the weight for control innervated muscles and are presented as mean ± s.e.m. $*P < 0.05$, $**P < 0.01$, independent-samples *t* test (two-tailed); $n = 4$ muscles for each condition. (**h**) Quantification of the cross-sectional area of EDL muscle expressed as percentage of the area in control innervated muscle; data are shown as mean ± s.e.m. $*P < 0.05$, independent-samples *t* test (two-tailed); myofibers of the entire muscle cross-section were analyzed, $n = 4$ muscles for each condition.

Gdf5 (BMP14) is required to prevent excessive muscle loss

To establish the protective role of BMPs during atrophy, we focused on BMP14 (encoded by *Gdf5*). Thus, we monitored denervation-induced atrophy in adult *Gdf5-bpJ*/*bpJ* mice[16], hereafter called $Gdf5^{-/-}$ mice. Because of chondrodysplasia in $Gdf5^{-/-}$ mice, distal muscles are smaller to various extents (EDL by 88%, tibialis anterior muscle by 60% and gastrocnemius muscle by 47% compared to comparable muscles in wild-type, control mice). However, $Gdf5^{-/-}$ muscles showed otherwise normal muscle architecture, normal vascularization, absence of inflammation and normal fiber size, suggesting that the abnormal development of these mice induced hypoplasia of distal muscles (**Supplementary Fig. 12**). Mutation of *Gdf5* blocked the activation of BMP signaling after denervation, as shown by the failure to increase expression of *Id1* and the levels of phosphorylated Smad1/5/8 (**Fig. 5d**,**e**). These findings confirm that activation of BMP signaling in denervated muscles is compromised in $Gdf5^{-/-}$ mice. Upon denervation, $Gdf5^{-/-}$ mice lost more muscle mass than age-matched control mice (**Fig. 5f**,**g**). Notably, different muscles from $Gdf5^{-/-}$ mice showed similar exacerbation of atrophy compared to comparable muscles in control mice. Consistent with morphology, quantification of cross-sectional area confirmed substantial atrophy in $Gdf5^{-/-}$ mice (**Fig. 5h** and **Supplementary Fig. 12c**), strongly suggesting that *Gdf5* (BMP14) is required to prevent excessive muscle loss upon denervation.

Muscle hypertrophy of $Mstn^{-/-}$ mice depends on BMP signaling

Data from $Smad4^{-/-}$ and $Gdf5^{-/-}$ muscles suggest that loss of BMP signaling exacerbates muscle atrophy and furthermore indicate that this pathway is dominant over myostatin signaling. To clarify this issue, we overexpressed noggin in the muscles of $Mstn^{-/-}$ mice, which are characterized by hypertrophy and hyperplasia (**Fig. 6**). Notably, inhibition of BMP signaling reverted the hypertrophic phenotype but not the hyperplasia of $Mstn^{-/-}$ muscles (**Fig. 6a**,**c**,**e**,**g**). Overexpression of noggin caused severe muscle wasting, both in $Mstn^{-/-}$ and control mice (29.4 mg and 15.6 mg of weight loss, respectively) (**Fig. 6c**). Noggin-mediated muscle wasting was due to atrophy (**Fig. 6e**,**g**) and not to myofiber loss (**Fig. 6g**). The decrease in fiber size was even more pronounced in $Mstn^{-/-}$ than in control mice (**Fig. 6g**). We next determined the function of myostatin and BMPs during denervation-induced

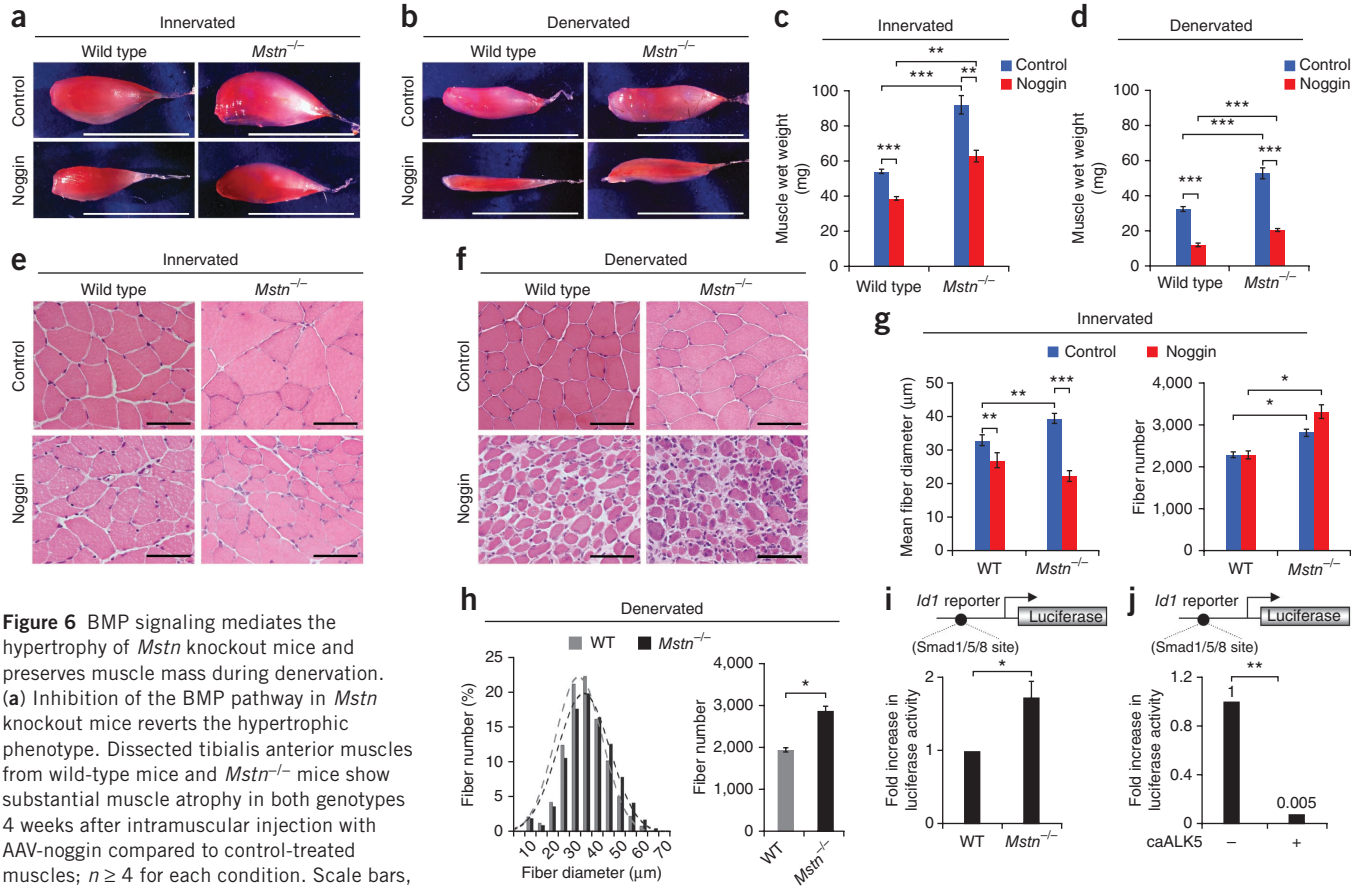

Figure 6 BMP signaling mediates the hypertrophy of *Mstn* knockout mice and preserves muscle mass during denervation. (**a**) Inhibition of the BMP pathway in *Mstn* knockout mice reverts the hypertrophic phenotype. Dissected tibialis anterior muscles from wild-type mice and $Mstn^{-/-}$ mice show substantial muscle atrophy in both genotypes 4 weeks after intramuscular injection with AAV-noggin compared to control-treated muscles; $n \geq 4$ for each condition. Scale bars, 1 cm. (**b**) Inhibition of the BMP pathway exaggerates muscle wasting during denervation. AAV-noggin and control-injected muscles were denervated 4 weeks after injection by neurectomy of the sciatic nerve, and mice were sacrificed after 2 further weeks. Dissected tibialis anterior muscles from wild-type mice and $Mstn^{-/-}$ mice are shown. Muscles were injected 4 weeks before denervation with control or AAV-noggin; $n \geq 4$ for each condition. Scale bars, 1 cm. (**c**) The diagram depicts the wet weights of the muscles in **a** and confirms that noggin induces muscle wasting in wild-type and $Mstn^{-/-}$ mice. Data are shown as mean ± s.e.m. $^{**}P < 0.01$, $^{***}P < 0.001$, independent-samples *t* test (two-tailed); $n \geq 4$ for each condition. (**d**) The wet weight of the muscles in **b** confirms the dramatic wasting of muscle tissue after noggin expression in denervated muscles. Data are shown as mean ± s.e.m. $^{***}P < 0.001$, independent-samples *t* test (two-tailed); $n \geq 4$ muscles for each condition. (**e**) Hematoxylin and eosin staining confirms that noggin overexpression causes myofiber atrophy; $n \geq 4$ muscles for each condition. Scale bars, 50 μm. (**f**) Hematoxylin and eosin staining shows the tremendous shrinkage of myofibers following noggin expression in denervated muscles from wild-type and $Mstn^{-/-}$ mice; $n \geq 4$ muscles for each condition. Scale bars, 50 μm. (**g**) Myofiber diameters and the number of myofibers were measured for infected fibers. Data are shown as mean ± s.e.m. $^{*}P < 0.05$, $^{**}P < 0.01$, $^{***}P < 0.001$; independent-samples *t* test (two-tailed); myofibers of the entire muscle cross-section were analyzed, $n = 4$ muscles for each condition. (**h**) Myofiber diameters and the number of myofibers were measured in denervated wild-type and $Mstn^{-/-}$ tibialis anterior muscle. Data are shown as mean ± s.e.m. $^{*}P < 0.05$, independent-samples *t* test (two-tailed); myofibers of the entire muscle cross-section were analyzed, $n = 4$ muscles for each condition. (**i**) Inhibition of myostatin pathways induces endogenous Smad1/5/8 activity on an *Id1* sensor. The *Id1* reporter was transfected into the tibialis anterior muscles of adult wild-type and $Mstn^{-/-}$ mice. Cotransfection with a *Renilla* luciferase vector was used to normalize for transfection efficiency. Seven days later, the ratio of firefly/*Renilla* luciferase activity was determined. Data are shown as mean ± s.d. $^{*}P < 0.05$, independent-samples *t* test (two-tailed); $n = 8$ muscles for each condition. (**j**) Activation of the myostatin pathway inhibits endogenous Smad1/5/8 activity on the *Id1* sensor. The *Id1* reporter was cotransfected into the tibialis anterior muscles of adult mice with vector expressing caALK5. Cotransfection with a *Renilla* luciferase vector was used to normalize for transfection efficiency. Seven days later, the ratio of firefly/*Renilla* luciferase activity was determined. Data are shown as mean ± s.d. $^{**}P < 0.01$, independent-samples *t* test (two-tailed); $n = 4$ muscles for each condition.

muscle atrophy. Two weeks after neurectomy, substantial muscle loss occurred in both wild-type and $Mstn^{-/-}$ mice. Denervation caused muscle atrophy without decreasing myofiber number, which remained higher in $Mstn^{-/-}$ muscles (**Fig. 6h**). Denervation also caused greater atrophy in muscles from $Mstn^{-/-}$ mice compared to wild-type mice (39.8 mg and 22.4 mg of weight loss, respectively). The final size of denervated myofibers was the same for the two genotypes, suggesting no protective effect of myostatin inhibition during denervation-induced atrophy (**Fig. 6f**,**h**), a finding that is consistent with the observed downregulation of *Mstn* and its receptor following denervation (**Fig. 5c** and **Supplementary Fig. 11**). Interestingly, the increased levels of phosphorylated Smad1/5/8 normally observed after denervation in wild-type muscles (**Fig. 5b**,**e**) were absent in $Mstn^{-/-}$ muscles (**Supplementary Fig. 13**), further strengthening the correlation between the absence of BMP signaling and greater atrophy.

To further investigate the protective role of BMP signaling in atrophying muscles, we overexpressed noggin in denervated muscles. Remarkably, noggin-mediated inhibition of BMPs resulted in particularly severe muscle atrophy after denervation (**Fig. 6b**,**d**,**f**). The loss of muscle mass mediated by noggin was even greater in $Mstn^{-/-}$ than in wild-type muscles (32.0 mg and 22.4 mg of weight loss, respectively) (**Fig. 6d**). Histological analyses confirmed that BMP inhibition caused

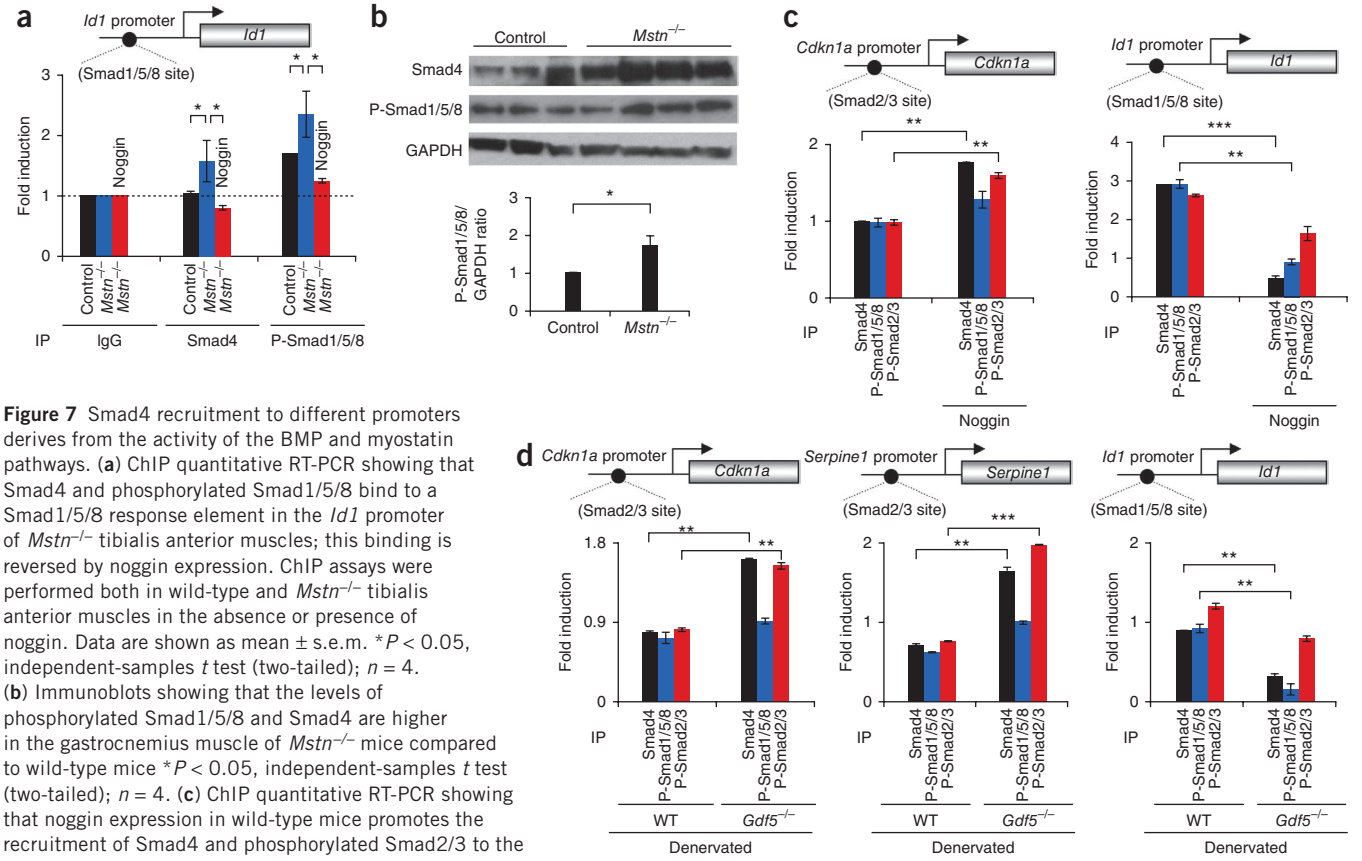

Figure 7 Smad4 recruitment to different promoters derives from the activity of the BMP and myostatin pathways. (**a**) ChIP quantitative RT-PCR showing that Smad4 and phosphorylated Smad1/5/8 bind to a Smad1/5/8 response element in the *Id1* promoter of *Mstn*$^{-/-}$ tibialis anterior muscles; this binding is reversed by noggin expression. ChIP assays were performed both in wild-type and *Mstn*$^{-/-}$ tibialis anterior muscles in the absence or presence of noggin. Data are shown as mean ± s.e.m. $*P < 0.05$, independent-samples *t* test (two-tailed); $n = 4$. (**b**) Immunoblots showing that the levels of phosphorylated Smad1/5/8 and Smad4 are higher in the gastrocnemius muscle of *Mstn*$^{-/-}$ mice compared to wild-type mice $*P < 0.05$, independent-samples *t* test (two-tailed); $n = 4$. (**c**) ChIP quantitative RT-PCR showing that noggin expression in wild-type mice promotes the recruitment of Smad4 and phosphorylated Smad2/3 to the *Cdkn1a* (p21) promoter and simultaneously results in the detachment of Smad4 and phosphorylated Smad1/5/8 from the *Id1* promoter. ChIP assays were performed in wild-type tibialis anterior muscles in the absence or presence of noggin. ChIP with IgG was used as the reference. Data are shown as mean ± s.e.m. $**P < 0.01$, $***P < 0.001$, independent-samples *t* test (two-tailed); $n = 3$. (**d**) ChIP quantitative RT-PCR showing that absence of *Gdf5* blunts the recruitment of Smad4 and phosphorylated Smad1/5/8 to the *Id1* promoter, whereas it induces the binding of Smad4 and phosphorylated Smad2/3 to the *Cdkn1a* (p21) and *Serpine1* (PAI-1) promoters. ChIP assays were performed in wild-type and *Gdf5*$^{-/-}$ denervated tibialis anterior muscles. Data are shown as mean ± s.e.m. $***P < 0.001$, $**P < 0.01$, independent-samples *t* test (two-tailed); $n = 3$.

severe atrophy that was more evident in *Mstn*$^{-/-}$ muscles (**Fig. 6f**). Conversely, expression of caALK3 in the tibialis anterior muscles of *Mstn*$^{-/-}$ mice by electroporation prevented muscle atrophy after denervation (**Supplementary Fig. 14**).

Smad4 recruitment is the limiting factor

Because Smad4 is the shared component of myostatin and BMP signaling, our data suggest that the balance between muscle atrophy and hypertrophy depends on the preferential recruitment of Smad4 to the myostatin versus the BMP pathway. In this scenario, myostatin can be envisioned as a factor that reduces the availability of Smad4 for BMP signaling. Indeed, the absence of myostatin led to significant activation of the Smad1/5/8 sensor (**Fig. 6i**). Conversely, sensor activity was greatly reduced when adult tibialis anterior muscles were transfected with vector expressing caALK5 (**Fig. 6j**). Notably, expression of BMPs, BMP receptors and Smad proteins did not change in *Mstn*$^{-/-}$ muscles (**Supplementary Fig. 15**).

Next, we monitored the recruitment of phosphorylated Smad1/5/8 and Smad4 to the *Id1* promoter (a Smad1/5/8 target) and the *Cdkn1a* promoter (p21, a Smad2/3 target) by chromatin immunoprecipitation (ChIP). ChIP quantitative RT-PCR showed increased binding of phosphorylated Smad1/5/8 and Smad4 on the *Id1* promoter but not on the *Cdkn1a* promoter in *Mstn*$^{-/-}$ compared to wild-type mice (**Fig. 7a** and **Supplementary Fig. 15**). Notably, noggin expression completely blocked the recruitment of phosphorylated Smad1/5/8 to the *Id1* promoter in *Mstn*$^{-/-}$ muscles (**Fig. 7a** and **Supplementary Fig. 15d**). Consistent with the results of *ID1* reporter and ChIP analyses, the levels of phosphorylation of Smad1/5/8 were found to be higher in myostatin-deficient muscles than in controls (**Fig. 7b**). Because we have shown that BMP signaling is active under physiological conditions, we monitored the recruitment of phosphorylated Smad2/3, phosphorylated Smad1/5/8 and Smad4 to the *Id1* and *Cdkn1a* promoters in wild-type muscles after noggin expression. Noggin completely abolished binding of phosphorylated Smad1/5/8 and Smad4 to the *Id1* promoter, whereas, simultaneously, it induced significant recruitment of phosphorylated Smad2/3 and Smad4 to the *Cdkn1a* promoter (**Fig. 7c**). Finally, we monitored binding of different Smad proteins in denervated tibialis anterior muscles from wild-type and *Gdf5*$^{-/-}$ mice. Absence of *Gdf5* led to a decrease in the binding of phosphorylated Smad1/5/8 and Smad4 to the *Id1* promoter (**Fig. 7d**) and led simultaneously to an increase in the binding of Smad4 and phosphorylated Smad2/3 to the promoters of *Cdkn1a* and *Serpine1* (encoding PAI-1, another Smad2/3 target) (**Fig. 7d**). Thus, our data are consistent with a model in which the BMP and myostatin pathways are in competition for Smad4.

The BMP-Smad1/5/8-Smad4 pathway negatively regulates MUSA1

To explain the dramatic atrophy present in denervated *Smad4*$^{-/-}$ and noggin-overexpressing muscles, we monitored the expression of

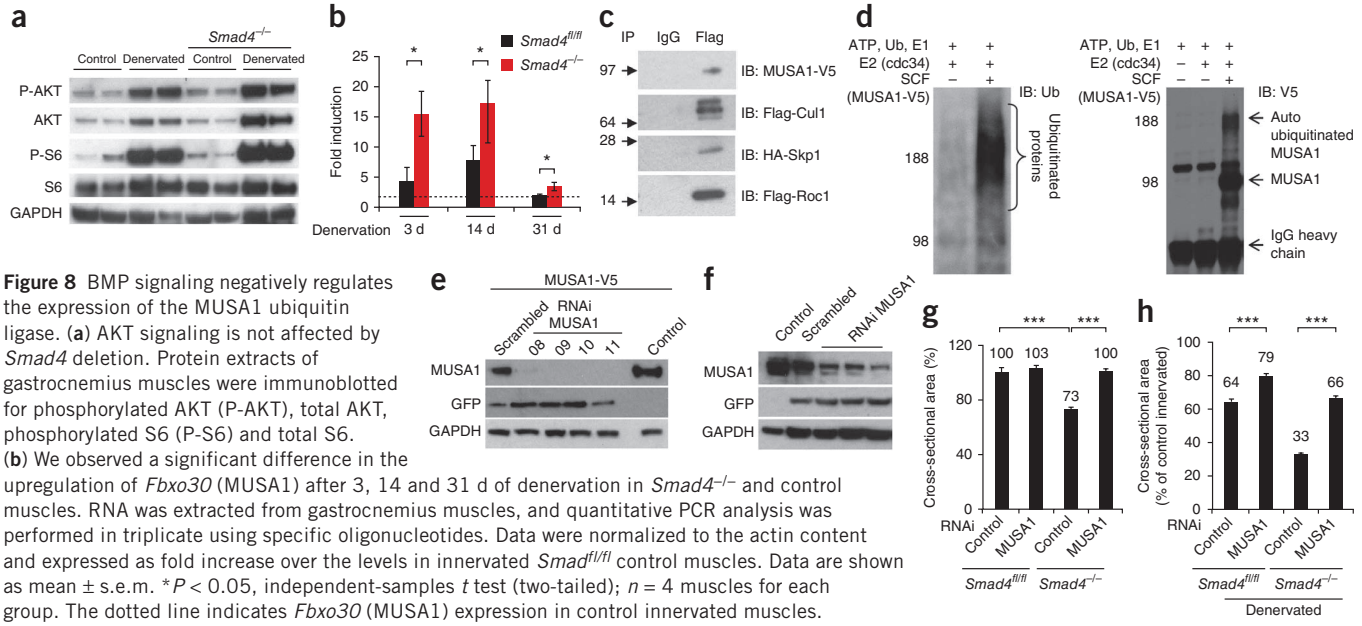

Figure 8 BMP signaling negatively regulates the expression of the MUSA1 ubiquitin ligase. (**a**) AKT signaling is not affected by *Smad4* deletion. Protein extracts of gastrocnemius muscles were immunoblotted for phosphorylated AKT (P-AKT), total AKT, phosphorylated S6 (P-S6) and total S6. (**b**) We observed a significant difference in the upregulation of *Fbxo30* (MUSA1) after 3, 14 and 31 d of denervation in *Smad4*$^{-/-}$ and control muscles. RNA was extracted from gastrocnemius muscles, and quantitative PCR analysis was performed in triplicate using specific oligonucleotides. Data were normalized to the actin content and expressed as fold increase over the levels in innervated *Smad*$^{fl/fl}$ control muscles. Data are shown as mean ± s.e.m. $^{*}P < 0.05$, independent-samples *t* test (two-tailed); $n = 4$ muscles for each group. The dotted line indicates *Fbxo30* (MUSA1) expression in control innervated muscles. (**c**) Coimmunoprecipitation experiment showing that MUSA1 is an F-box protein that forms an SCF complex. C2C12 muscle cell lines were transfected with plasmids expressing MUSA1, Skp1, Cul1 and Roc1. After 24 h, cells were lysed, and immunoprecipitation (IP) against the Flag tag or control IgG was performed. The results of immunoblotting (IB) for the different SCF components are shown. (**d**) Purified SCF complexes containing MUSA1-V5 are active in catalyzing autoubiquitination. *In vitro* ubiquitination reactions were carried out by incubating the MUSA1-V5–containing affinity-purified SCF complexes with recombinant E1 and E2 enzymes, ubiquitin (Ub) and ATP at 37 °C for 5 h. Mixtures were then subjected to SDS-PAGE, and immunoblotting with antibodies to ubiquitin and V5 was performed. This E3 ligase activity requires neddylation of MUSA1-V5, as it was only observed after purification with o-phenanthroline to inhibit cullin deneddylation. Right, autoubiquitination activity of MUSA1. (**e**) RNAi-mediated knockdown of MUSA1 shown by immunoblotting. MEFs were transfected with vectors expressing different shRNAs against *Fbxo30* (MUSA1) together with vector encoding mouse MUSA1-V5. (**f**) shRNAs efficiently knocks down MUSA1 protein *in vivo*. Oligo 10 was transfected by electroporation into tibialis anterior muscles. Two weeks later, muscles were collected and frozen. Cryosections of the transfected area were lysed and immunoblotted for MUSA1. (**g**) Inhibition of MUSA1 rescues atrophy in *Smad4*$^{-/-}$ muscles but does not affect wild-type muscles. Adult muscle fibers were cotransfected with bicistronic expression vectors that encode shRNAs against *Fbxo30* (MUSA1) or scrambled shRNA and GFP and were denervated. Two weeks later, cross-sectional area of transfected fibers, identified by GFP fluorescence, were measured; data are shown as mean ± s.e.m. $^{***}P < 0.001$, independent-samples *t* test (two-tailed); $n = 6$ muscles for each group. (**h**) Inhibition of MUSA1 prevents muscle atrophy in denervated *Smad4*$^{-/-}$ and wild-type muscles. Data are shown as mean ± s.e.m. $^{***}P < 0.001$, independent-samples *t* test (two-tailed); $n = 6$ muscles for each group.

atrophy-related genes[17–19], including ubiquitin ligases *Fbxo32* (atrogin-1) and *Trim63* (MuRF1) and autophagy-related genes *Ctsl* (cathepsin L), *Map1lc3b* (LC3b), *Becn1* (beclin 1) and *Bnip3*. The expression of these atrophy-related genes showed no or minor changes between *Smad4*$^{fl/fl}$ and *Smad4*$^{-/-}$ muscles after 3, 14 and 31 d of denervation (**Supplementary Fig. 16**). Therefore, they are unlikely to be responsible for the dramatic muscle atrophy in *Smad4*$^{-/-}$ mice. Moreover, overexpression of noggin in the denervated muscles of control mice did not enhance expression of these genes (**Supplementary Fig. 17**). Because the proteolysis of contractile proteins is controlled by the ubiquitin-proteasome system, we sought to better characterize the involvement of atrogin-1 and MuRF1 in the atrophy of denervated *Smad4*$^{-/-}$ muscle by knocking down these ubiquitin ligases. Several shRNAs were tested, and two that efficiently reduced the levels of *Fbxo32* (atrogin-1) and *Trim63* (MuRF1) transcripts *in vivo* were used for subsequent studies (**Supplementary Fig. 18**). Knocking down atrogin-1 or MuRF1 did not affect fiber size in control, innervated muscles, nor did it revert the atrophy present in *Smad4*$^{-/-}$ muscles (**Supplementary Fig. 19a**,**c**). In agreement with previous findings on MuRF1 and atrogin-1 knockout mice[20], inhibition of both ubiquitin ligases reduced muscle atrophy after denervation, yet the degree of this sparing effect was similar between control and *Smad4*$^{-/-}$ mice (**Supplementary Figs. 19b**,**d** and **20**). In line with a recent report on atrogin-1 knockout mice[21], knocking down atrogin-1 after denervation triggered myofiber degeneration and inflammation in both control and *Smad4*$^{-/-}$ mice (**Supplementary Fig. 19e**,**f**). Notably, the large fibers in denervated muscles were always positive for immunoglobulins, a marker of necrosis (**Supplementary Fig. 19f**), confirming that the increase in size is due to cellular swelling as a consequence of membrane ruptures and water influx.

These data suggest that Smad4-dependent transcription controls a different set of genes that can modulate the proteolytic machinery. We and others have shown that the myostatin pathway impinges on insulin-like growth factor 1 (IGF1)-AKT signaling[5,6]. Thus, we hypothesized that atrophy was due to a decrease in the anabolic AKT-mTOR pathway. However, *Smad4*-null muscles did not display any significant difference in the IGF1 pathway, suggesting that the excessive atrophy after 14 d of denervation is not caused by AKT suppression (**Fig. 8a** and **Supplementary Fig. 21a**).

To determine how the reduction in BMP-Smad1/5/8-Smad4 signaling affects protein breakdown, we studied the progressive atrophy that occurs in *Smad4*$^{-/-}$ muscles. As shown in **Figure 2b**, atrophy stops after 14 d of denervation in control mice yet continues in *Smad4*$^{-/-}$ mice (**Fig. 2b** and **Supplementary Fig. 3a–c**). This finding suggests that genes involved in protein breakdown are still active in *Smad4*$^{-/-}$ mice past 14 d. We performed gene expression profiling on muscles from *Smad4*$^{-/-}$ and control mice that had been innervated or denervated for 14 d, focusing on genes that were differentially upregulated in denervated *Smad4*$^{-/-}$ muscles compared to in control muscles.

Among the various genes, our attention was drawn to a gene that encodes a previously uncharacterized F-box protein (Fbxo30) belonging to the SCF complex family of ubiquitin ligases[22]. We confirmed that expression of *Fbxo30* was induced in denervated muscles and that it was significantly upregulated in the atrophying muscles of *Smad4*-deficient mice. Moreover, its expression was still higher 30 d after denervation in $Smad4^{-/-}$ compared to $Smad4^{fl/fl}$ mice (**Fig. 8b**). We named the protein encoded by this gene muscle ubiquitin ligase of SCF complex in atrophy-1 (MUSA1). Notably, noggin overexpression in denervated muscles significantly enhanced *Fbxo30* (MUSA1) expression, confirming that *Fbxo30* is negatively regulated by the BMP pathway (**Supplementary Fig. 17**). MUSA1 expression was higher in $Smad4^{-/-}$ than in $Smad4^{fl/fl}$ muscle (**Supplementary Fig. 21b–d**). Notably, denervation significantly increased MUSA1 protein levels in muscles from $Smad4^{fl/fl}$ and $Smad4^{-/-}$ mice, albeit to a lesser extent than it increased transcript levels (**Supplementary Fig. 21c,d**). Denervated *Smad4*-deficient fibers showed precocious upregulation and higher levels of MUSA1 protein than denervated control fibers (**Supplementary Fig. 21d**). Immunoprecipitation experiments confirmed that MUSA1 forms an SCF complex with Skp1, Cullin1 and Roc1 (**Fig. 8c**). *In vitro* ubiquitination assays showed an increase in ubiquitinated proteins when MUSA1 protein was added to the reaction (**Fig. 8d**, left). Moreover, similar to other E3 ligases of the SCF complex, MUSA1 underwent autoubiquitination (**Fig. 8d**, right). Altogether, these findings confirm that MUSA1 is a ubiquitin ligase of the SCF family.

To establish the physiological relevance of this ubiquitin ligase in atrophy, we knocked down MUSA1 in tibialis anterior muscles *in vivo*. We tested four different shRNAs to specifically reduce MUSA1 protein levels (**Fig. 8e**), all of which efficiently knocked down MUSA1. We then transfected oligo 11 into the innervated and denervated muscles of $Smad4^{fl/fl}$ and $Smad4^{-/-}$ mice. MUSA1 protein levels were successfully reduced by oligo 11 *in vivo* (**Fig. 8f**). Whereas MUSA1 knockdown *in vivo* did not affect the fiber size of control innervated muscles, it completely restored the size of *Smad4*-deficient muscles to normal (**Fig. 8g**). Notably, MUSA1 inhibition significantly protected denervated muscles from atrophy (**Fig. 8h**), and the drastic atrophy seen in *Smad4*-deficient muscles was blunted (**Fig. 8h**). These effects of MUSA1 inhibition on both innervated and denervated $Smad4^{-/-}$ fibers are very different from the inability of atrogin-1 and MuRF1 inhibition to restore normal fiber size or to prevent excessive muscle loss after denervation (compare **Fig. 8g,h** with **Supplementary Fig. 19a–d**). Finally, overexpression of MUSA1 in tibialis anterior muscles, similar to overexpression of atrogin-1 and MuRF1 (ref. 23), did not induce muscle atrophy under normal physiological conditions (**Supplementary Fig. 22**). In conclusion, we have identified MUSA1 as a critical protein under BMP regulation whose induction is required for atrophy.

DISCUSSION

This study provides several new insights into signaling by TGF-β pathways and their contribution to the regulation of muscle mass in adulthood. The most striking conclusion is that BMP signaling is the dominant pathway controlling muscle mass, even more so than myostatin. In particular, we show that the hypertrophic phenotype caused by myostatin inhibition in fact results from unrestrained BMP signaling. Our data fit with a model in which a decrease in the levels of phosphorylated Smad2/3 leads to the release of Smad4, which is recruited into BMP signaling to promote hypertrophy and counteract atrophy. Conversely, when the BMP pathway is blocked or myostatin expression is increased, more Smad4 is available for phosphorylated Smad2/3, leading to an atrophy response. Therefore, under normal circumstances, a balance between these competing pathways is required to maintain muscle mass. The dramatic loss of muscle mass after denervation in *Smad4* knockout mice and following overexpression of noggin strongly suggests that BMP signaling is also required to prevent excessive muscle loss under pathological conditions. Similar conclusions have been reached by an independent study on BMP signaling in skeletal muscle[24]. The molecular mechanism underlying the anti-atrophic action of the BMP pathway relies on the negative effect it exerts on the expression of a newly characterized ubiquitin ligase that we named MUSA1. This E3 ligase is not only required for protein breakdown in atrophying muscles but also exacerbates muscle atrophy in *Smad4*-deficient mice. Similar to other E3 ligases, MUSA1 undergoes autoubiquitination. Thus, it is reasonable to suggest that increased ligase activity of MUSA1 during denervation would amplify its autoubiquitination activity, resulting in increased proteasome-dependent degradation. Therefore, transcriptional upregulation is particularly important, mostly to replenish the loss of MUSA1 protein that occurs in denervated muscles as a consequence of increased MUSA1 activity.

Mutations in the *SMAD4* gene in humans result in Myhre syndrome, which is characterized by increased muscle mass[25], thus contrasting with the muscle atrophy observed in our $Smad4^{-/-}$ mice. However, owing to the lack of any histological analysis on muscle biopsies from individuals with Myhre syndrome, it is unclear whether the larger muscles described in these individuals are due to hyperplasia or hypertrophy. Moreover, molecularly, Myhre syndrome differs substantially from *Smad4* deficiency. In Myhre syndrome, *SMAD4* mutations stabilize SMAD4 protein, inducing higher levels of expression in affected individuals. The lack of a protein implies a very different outcome than the persistence of a mutated protein in terms of loss or gain of function. In fact, mutations that lead to protein accumulation may promote new roles for that protein, in this instance promoting SMAD4 to act as a sponge for cofactors and/or transcription factors, thus affecting different signaling pathways and biological processes. Interestingly, missense mutations in *SMAD4* caused an increase in the levels of phosphorylated SMAD2/3 and phosphorylated SMAD1/5/8 in individuals with Myhre syndrome, who showed different ability to trigger SMAD-dependent transcription. In fact, cells from individuals with Myhre syndrome showed strong downregulation of all myostatin target genes studied, whereas this was not the case for BMP targets, whose expression was more variable, with some being downregulated and others being upregulated[25]. Therefore, it appears that the hypertrophic phenotype associated with Myhre syndrome is characterized by inhibition of myostatin signaling but not of the BMP pathway.

In conclusion, BMP signaling is indispensable for the regulation of adult muscle mass in normal and pathological situations, highlighting its importance in developing new strategies for controlling protein breakdown and for treating muscle-wasting disorders.

METHODS

Methods and any associated references are available in the online version of the paper.

Accession codes. Gene expression profiling data have been deposited in the NCBI Gene Expression Omnibus (GEO) and are available under accession GSE49826.

Note: Any Supplementary Information and Source Data files are available in the online version of the paper.

ACKNOWLEDGMENTS

We gratefully acknowledge the critical reading of K. Dyar. We thank S.-J. Lee (Johns Hopkins University School of Medicine) for the kind gift of *Mstn*$^{-/-}$ mice and S.J. Burden (Skirball Institute, New York University Medical School) for the gift of MLC1f-Cre mice. HA-Skp1, Flag-Cul1 and Flag-Roc1 were kindly provided by S.H. Lecker. We acknowledge C. Beley and G. Precigout for AAV production. This work was supported by Telethon Italy (TCP04009), by the European Research Council (ERC; 282310-MyoPHAGY), by the European Union (MYOAGE, contract 223576 of Framework Programme 7), by the Leducq Foundation and by the Italian Ministry of Education (MiUR; PRIN 2010/2011) to M.S., by Associazione Italiana per la Ricerca sul Cancro (AIRC) Investigator grants to S.P. and S.D. and by a Comitato Promotore Telethon Grant, the AIRC Special Program Molecular Clinical Oncology "5 per Mille," HSFP, Excellence-IIT and Epigenetics Flagship project CNR-MiUR grants to S.P., by the Association Française contre les Myopathies to H.A., E.S., A.S. and A.F., by the Agence Nationale de la Recherche to H.A. (ANR-12-BSV1-0038) and by the Deutsche Forschungsgemeinschaft and the Université Franco-Allemand (as part of the MyoGrad International Graduate School for Myology GK 1631/1 and CDFA-06-11) to S.S., H.A., A.S. and E.S. E.E. is the recipient of a CARIPARO Foundation PhD fellowship.

AUTHOR CONTRIBUTIONS

R.S. and S.B. performed biochemical analyses, RNA analysis, muscle transfections, mouse treatments, ChIP analysis and cloning. M.S. performed electron microscopy. R.S., S.B. and E.S. performed histology. E.S., A.S., H.A. and E.M. performed AAV infection, morphological and immunohistochemical analysis, protein analysis and RNA analysis. B.B. and L.T. analyzed muscle mechanics. J.Z. performed *in vitro* ubiquitination assays and analysis. E.E. and E.S. genotyped and maintained mice. S.S. provided *Gdf5*-mutant mice. A.F. and R.S. performed denervation experiments. R.S., E.S., H.A., M.S., S.D., S.P., E.M., B.B. and A.L.G. were involved in data analysis. R.S., E.S., M.S., H.A., S.D. and S.P. designed the study, analyzed the data and wrote the manuscript. All authors discussed the results and commented on the manuscript.

COMPETING FINANCIAL INTERESTS

The authors declare no competing financial interests.

1. Sartorelli, V. & Fulco, M. Molecular and cellular determinants of skeletal muscle atrophy and hypertrophy. *Sci. STKE* **2004**, re11 (2004).
2. Sandri, M. Signaling in muscle atrophy and hypertrophy. *Physiology* (*Bethesda*) **23**, 160–170 (2008).
3. Lee, S.J. & McPherron, A.C. Regulation of myostatin activity and muscle growth. *Proc. Natl. Acad. Sci. USA* **98**, 9306–9311 (2001).
4. Lee, S.J. *et al.* Regulation of muscle growth by multiple ligands signaling through activin type II receptors. *Proc. Natl. Acad. Sci. USA* **102**, 18117–18122 (2005).
5. Sartori, R. *et al.* Smad2 and 3 transcription factors control muscle mass in adulthood. *Am. J. Physiol. Cell Physiol.* **296**, C1248–C1257 (2009).
6. Trendelenburg, A.U. *et al.* Myostatin reduces Akt/TORC1/p70S6K signaling, inhibiting myoblast differentiation and myotube size. *Am. J. Physiol. Cell Physiol.* **296**, C1258–C1270 (2009).
7. Walsh, D.W., Godson, C., Brazil, D.P. & Martin, F. Extracellular BMP-antagonist regulation in development and disease: tied up in knots. *Trends Cell Biol.* **20**, 244–256 (2010).
8. Miyazono, K. & Miyazawa, K. Id: a target of BMP signaling. *Sci. STKE* **2002**, pe40 (2002).
9. Yu, P.B. *et al.* BMP type I receptor inhibition reduces heterotopic ossification. *Nat. Med.* **14**, 1363–1369 (2008).
10. Dennler, S. *et al.* Direct binding of Smad3 and Smad4 to critical TGF β–inducible elements in the promoter of human plasminogen activator inhibitor–type 1 gene. *EMBO J.* **17**, 3091–3100 (1998).
11. Korchynskyi, O. & ten Dijke, P. Identification and functional characterization of distinct critically important bone morphogenetic protein–specific response elements in the *Id1* promoter. *J. Biol. Chem.* **277**, 4883–4891 (2002).
12. Lecker, S.H., Goldberg, A.L. & Mitch, W.E. Protein degradation by the ubiquitin-proteasome pathway in normal and disease states. *J. Am. Soc. Nephrol.* **17**, 1807–1819 (2006).
13. Romanello, V. *et al.* Mitochondrial fission and remodelling contributes to muscle atrophy. *EMBO J.* **29**, 1774–1785 (2010).
14. Zimmerman, L.B., De Jesus-Escobar, J.M. & Harland,, R.M. The Spemann organizer signal noggin binds and inactivates bone morphogenetic protein 4. *Cell* **86**, 599–606 (1996).
15. Krause, C., Guzman, A. & Knaus, P. Noggin. *Int. J. Biochem. Cell Biol.* **43**, 478–481 (2011).
16. Storm, E.E. *et al.* Limb alterations in brachypodism mice due to mutations in a new member of the TGF-β superfamily. *Nature* **368**, 639–643 (1994).
17. Mammucari, C. *et al.* FoxO3 controls autophagy in skeletal muscle *in vivo*. *Cell Metab.* **6**, 458–471 (2007).
18. Sacheck, J.M. *et al.* Rapid disuse and denervation atrophy involve transcriptional changes similar to those of muscle wasting during systemic diseases. *FASEB J.* **21**, 140–155 (2007).
19. Sandri, M. *et al.* Foxo transcription factors induce the atrophy-related ubiquitin ligase atrogin-1 and cause skeletal muscle atrophy. *Cell* **117**, 399–412 (2004).
20. Bodine, S.C. *et al.* Identification of ubiquitin ligases required for skeletal muscle atrophy. *Science* **294**, 1704–1708 (2001).
21. Gomes, A.V. *et al.* Upregulation of proteasome activity in muscle RING finger 1–null mice following denervation. *FASEB J.* **26**, 2986–2999 (2012).
22. Lipkowitz, S. & Weissman, A.M. RINGs of good and evil: RING finger ubiquitin ligases at the crossroads of tumour suppression and oncogenesis. *Nat. Rev. Cancer* **11**, 629–643 (2011).
23. Hirner, S. *et al.* MuRF1-dependent regulation of systemic carbohydrate metabolism as revealed from transgenic mouse studies. *J. Mol. Biol.* **379**, 666–677 (2008).
24. Winbanks, C.E. *et al.* The Bone Morphogenetic Protein (BMP) axis is a positive regulator of skeletal muscle mass. *J. Cell Biol.* (in the press).
25. Le Goff, C. *et al.* Mutations at a single codon in Mad homology 2 domain of *SMAD4* cause Myhre syndrome. *Nat. Genet.* **44**, 85–88 (2012).

ONLINE METHODS

Generation of muscle-specific *Smad4* knockout mice. Mice bearing *Smad4* floxed alleles[26] (*Smad4*$^{fl/fl}$) were crossed with transgenic mice expressing Cre under the control of a myosin light chain 1 fast promoter (*Myl1-cre*)[17,27]. Genomic DNA isolated from *Smad4*$^{fl/fl}$ mice was subjected to PCR analysis. Cre-mediated recombination was confirmed by PCR with genomic DNA from gastrocnemius muscles. The primers used to detect the *Smad4*-null allele are listed in **Supplementary Table 1**. Experiments were performed on 2- to 3-month-old male and female mice; mice of the same sex and age were used for each individual experiment.

Mice and *in vivo* transfection experiments. Mice were handled by specialized personnel under the control of inspectors of the Veterinary Service of the Local Sanitary Service (ASL 16–Padova), the local officers of the Ministry of Health. All procedures are specified in the projects approved by the Italian Ministero Salute, Ufficio VI (authorization number C65). All experiments were performed on adult, 2-month-old male CD1 mice (28–32 g). *In vivo* transfection experiments were performed by intramuscular injection of expression plasmids in tibialis anterior muscle followed by electroporation as previously described[19]. Denervation was performed by cutting the sciatic nerve of the left limb, while the right limb was used as the control. Muscles were removed at various time points after transfection and frozen in liquid nitrogen for subsequent analyses.

Mstn$^{+/+}$ and *Mstn*$^{-/-}$ mice on a C57BL/6J background[28] were generated using a heterozygous mating system in the animal facilities of the Pierre et Marie Curie Medical Faculty (Paris, France) and were kept according to institutional guidelines. Experiments were performed on 3- to 4-month-old male and female mice; mice of the same sex were used for each individual experiment. Investigations of mice were carried out under the respective laboratory and animal facility license A75-13-11 and in compliance with the guide *Experimentation Animale du CIUP*. Some C57BL/6J control mice (*Mstn*$^{+/+}$) were purchased from Charles River. *Gdf5-bpJ/bpJ* (BMP14) mutant mice have been described previously[16] and were maintained in a homozygous mating system; control mice were of the corresponding A/J genetic background and were purchased from Harlan. Experiments were performed on 3- to 5-month-old male mice.

AAV production. The noggin construct, prepared by PCR amplification of chick cDNA using the primers listed in **Supplementary Table 1**, was subcloned into the pCR2.1-TOPO plasmid vector (TOPO Cloning, Life Technologies) and then introduced into an AAV-2–based vector between the two inverted terminal repeats and under the control of the cytomegalovirus (CMV) promoter using the XhoI and EcoRI sites. AAV2/1-noggin (AAV-noggin) was produced in human embryonic kidney 293 cells by the triple-transfection method using the calcium phosphate precipitation technique with both the pAAV2 propeptide plasmid, the pXX6 plasmid coding for the adenoviral sequences essential for AAV production and the pRepCAp plasmid coding for AAV1. Virus was then purified by two cycles of cesium chloride gradient centrifugation and was concentrated by dialysis. Final viral preparations were kept in PBS at −80 °C. Particle titer (number of viral genomes) was determined by quantitative PCR.

AAV2/1 vectors encoding caALK3 (ref. 29) and a non-functional construction U7-c (AAV-caALK3 and AAV-control, respectively) were prepared using the same protocol as for AAV-noggin. caALK3 was introduced into an AAV-2–based vector between the two inverted terminal repeats and under the control of the CMV promoter using the MluI and XhoI sites.

AAV injection. The quantity of AAV used for intramuscular delivery was calculated according to total body weight (x µl = 1.5 × body weight (g)) and was about 30–50 µl. AAV was injected into the muscles of the anterior compartment of the lower leg (tibialis anterior and EDL muscles) of 3- to 4-month-old *Mstn*$^{-/-}$ and *Mstn*$^{+/+}$ mice. In control experiments, either AAV-control or PBS was used for injection (n = 4 for each condition). Comparison of muscle size, histology and fiber size did not show differences in wild-type tibialis anterior muscles after injection with AAV-control or PBS, especially after denervation. AAV-noggin was used at 1.2×10^{12} or 1.9×10^{13} vg/ml, AAV-caALK3 was used at 1.3×10^{12} or 1.87×10^{12} viral genomes (vg)/ml, and AAV-control was used at 1.6×10^{12}, 1.2×10^{12} or 7.44×10^{12} vg/ml.

Denervation experiments. Four weeks after injection of mice with AAV or control, the sciatic nerve was neuroectomized (ablation of a 5-mm segment of the sciatic nerve) under general anesthesia (pentobarbital sodium, 50 mg/kg). Mice were sacrificed 2 weeks after denervation, and the muscles of the anterior compartment of the lower leg were dissected, weighed and thereafter frozen in liquid nitrogen or in isopentane precooled in liquid nitrogen and stored at −80 °C until histology or molecular analysis.

Gene expression analyses. Total RNA was prepared from tibialis anterior muscles using the Promega SV Total RNA Isolation kit. cDNA generated with Life Technologies SuperScript III Reverse Transcriptase was analyzed by quantitative RT-PCR using the Qiagen QuantiTect SYBR Green PCR kit. All data were normalized to *Gapdh* and *Actb* expression levels. The sequences of the oligonucleotide primers used are shown in **Supplementary Table 2**.

Plasmids and antibodies for immunoblotting. Transfection experiments used the following constructs: pGL3(CAGA)12-luc[10]; ID1-luc[11]; pRL-TK (Promega); pCS4+ (a kind gift of M. Whitman); ca-hALK5 (pcDNA3-HASL-ALK5(T204D)); ca-mALK3/BMPR1A (pCS2+-BMPRI(Q233D3S)); pEGFP-C1 (Clontech); HA-Skp1; Flag-Cul1; and Flag-Roc1. For the preparation of the mSmad1-V5 and mFbxo30/MUSA1-V5 expression constructs, muscle cDNA was amplified by PCR using the primers listed in **Supplementary Table 1**.

Amplified sequence was cloned into the pcDNA3.1/V5-His TOPO TA (Life Technologies) expression vector and sequenced. RNAi-mediated knockdown was carried out by cotransfection with shRNA constructs (**Supplementary Table 3**).

The following antibodies from Cell Signaling Technology were used: rabbit polyclonal antibody to Akt (9272), rabbit polyclonal antibody to phosphorylated Akt (Ser473) (9271), rabbit polyclonal antibody to phosphorylated S6 ribosomal protein (Ser240/244) (2215), rabbit monoclonal antibody to S6 ribosomal protein (5G10) (2217), rabbit polyclonal antibody to phosphorylated Smad1 (Ser463/465)/Smad5 (Ser463/465)/Smad8 (Ser426/438) (9511) and rabbit polyclonal antibody to phosphorylated Smad3 (Ser423/425) (9514). From Santa Cruz Biotechnology, the following antibodies were used: antibody to Smad4 (B-8) (sc-7966), antibody to GFP (sc-8334) and antibody to FBXO30 (N-13) (sc-138935). Mouse monoclonal antibodies to Flag (M2; F3165), HA (H3663) and actin (A4700) were purchased from Sigma. Mouse monoclonal antibody to V5 and rabbit polyclonal antibody to phosphorylated Smad2 (44-244G) were purchased from Life Technologies. Rabbit polyclonal antibody to atrogin-1 (AP2041) and mouse monoclonal antibody to GAPDH (ab8245) were purchased from ECM Biosciences and Abcam, respectively.

Cell culture and transient transfection. MEFs or the C2C12 muscle cell line were purchased from ATCC and were cultured in DMEM (Gibco–Life Technologies) supplemented with 10% FCS and 1% penicillin-streptomycin mixture at 37 °C and 5% CO_2 until cells reached confluence. Cells were transfected using Lipofectamine 2000 (Life Technologies) according to the manufacturer's instructions. Cell lines used in the experiments were authenticated and tested for mycoplasma contamination.

RNAi *in vivo*. *In vivo* RNAi experiments were performed as previously described[19] using at least three different sequences for each gene. The sequences used are given in **Supplementary Table 3**. For the validation of shRNA constructs, MEFs were maintained in DMEM supplemented with 10% FBS and were transfected with shRNA constructs using Lipofectamine 2000. Cells were lysed 24 h later, and immunoblotting was performed.

ChIP assays. We performed ChIP assays in adult skeletal muscles using the Chromatin Immunoprecipitation (ChIP) assay kit (Upstate) as previously described[17,30]. Soluble chromatin was coimmunoprecipitated with rabbit polyclonal antibody to Smad4 (H-552) (sc-7154-X, Santa Cruz Biotechnology), rabbit polyclonal antibody to phosphorylated Smad1/5/8 (9511, Cell Signaling Technology), rabbit polyclonal antibody to phosphorylated Smad2/3 (Ser423/435) (sc-11769-X, Santa Cruz Biotechnology) or an equal amount of normal rabbit IgG (sc-2027, Santa Cruz Biotechnology). After reversal of DNA cross-linking, samples were subjected to quantitative RT-PCR. The sequences for the oligonucleotide primers used are shown in **Supplementary Table 4**. The regions of amplification contained the Smad1/5/8 binding sites in the *Id1*

promoter[11] and the Smad2/3 binding sites in the *Serpine1* (PAI-1) and *Cdkn1a* (p21) promoters[10,31].

Gene expression profiling. Total RNA was prepared from gastrocnemius muscles using TRIzol (Life Technologies) following the manufacturer's instructions. Next, a clean-up step and on-column DNase I treatment were performed using the RNeasy Fibrous Tissue Mini kit (Qiagen). RNA was quantified using a NanoDrop ND-1000 spectrophotometer, and quality was monitored with the Agilent 2100 Bioanalyzer (Agilent Technologies). Cy3-labeled cRNA was prepared from 1 µg of RNA using One-Color Microarray-Based Gene Expression Analysis (Quick Amp Labeling) (Agilent Technologies) according to the manufacturer's instructions, and RNeasy column purification was performed (Qiagen). Dye incorporation and cRNA yield were checked with the NanoDrop ND-1000 Spectrophotometer. Cy3-labeled cRNA (1.65 µg; specific activity of >9.0 pmol Cy3/µg of cRNA) was fragmented at 60 °C for 30 min in a reaction volume of 55 µl containing 1× Agilent fragmentation buffer and 2× Agilent blocking agent, following the manufacturer's instructions. On completion of the fragmentation reaction, 55 µl of 2× GEx Hybridization buffer HI-RPM was added to the fragmentation mixture, and mixtures were hybridized to Agilent Whole-Mouse Genome Oligo Microarrays (G4122F) for 17 h at 65 °C in a rotating Agilent hybridization oven. After hybridization, microarrays were washed 1 min at room temperature with GE Wash Buffer 1 (Agilent Technologies) and 1 min at 37 °C with GE Wash buffer 2 (Agilent Technologies) and then dried. Slides were scanned immediately after washing on the Agilent DNA Microarray Scanner (G2505B) using the one-color scan setting for 1 × 44 k array slides (scan area of 61 × 21.6 mm; scan resolution of 5 µm; dye channel set to green; green PMT set to 100%). Scanned images were analyzed with Feature Extraction Software 10.5.1.1 (Agilent Technologies) using default parameters (protocol GE1_107_Sep09 and Grid: 014868_D_20070820) to obtain background-subtracted and spatially detrended Processed Signal intensities. Signal intensities were normalized using quantile normalization. Lists of differentially expressed genes are presented in **Supplementary Tables 5** and **6**.

Immunoblotting and immunoprecipitation. Frozen gastrocnemius muscles were powdered by mortar and pestle and lysed in a buffer containing 50 mM Tris, pH 7.5, 150 mM NaCl, 5 mM $MgCl_2$, 1 mM DTT, 10% glycerol, 2% SDS, 1% Triton X-100, Roche Complete Protease Inhibitor Cocktail, 1 mM PMSF, 1 mM $NaVO_3$, 5 mM NaF and 3 mM β-glycerophosphate. The lysis buffer used for MEFs contained 50 mM Tris, pH 7.5, 150 mM NaCl, 5 mM $MgCl_2$, 1 mM DTT, 10% glycerol, 1 mM EDTA, 0.5% Triton X-100 and the protease inhibitors listed above. Alternatively, lysis buffer contained 50 mM Tris-HCl, pH 7.2, 250 mM NaCl, 2% NP-40, 0.1% SDS, 0.5% sodium deoxycholate and 2.5 mM EDTA, pH 8, with phosphatase and protease inhibitors. For nuclear protein extraction, lysis buffer contained 20 mM HEPES, pH 7.9, 5 mM NaF, 1 mM Na_2MoO_4, 0.1 mM EDTA and 0.5% NP-40. Samples were immunoblotted as previously described[19] and visualized with SuperSignal West Pico Chemiluminescent substrate (Pierce). Blots were stripped using Restore Western Blotting Stripping Buffer (Pierce) according to the manufacturer's instructions and were reprobed if necessary.

For coimmunoprecipitation, C2C12 muscle cell lines were transfected with expression plasmids for MUSA1-V5, HA-Skp1, Flag-Cul1 and Flag-Roc1. After 24 h, cells were lysed in a buffer containing 50 mM Tris, pH 7.5, 100 mM NaCl, 5 mM $MgCl_2$, 1 mM DTT, 0.5% Triton X-100 and protease and phosphatase inhibitors. Total protein (1 mg) was incubated with 10 µg of the mouse monoclonal antibody to Flag or with non-specific mouse IgG along with 30 µl of Protein A/G PLUS-Agarose (sc-2003, Santa Cruz Biotechnology) overnight at 4 °C with rotating. Beads were then washed three times with PBS plus Roche Complete Protease Inhibitor Cocktail 1×. Beads were finally resuspended in 30 µl of LDS Sample Buffer 1× (NuPAGE Life Technologies) and 50 mM DTT, and samples were boiled at 95 °C for 5 min and analyzed by immunoblotting.

***In vitro* ubiquitination.** HEK293 cells stably expressing V5-tagged MUSA1 were established. To isolate MUSA1-V5–containing SCF complexes, five 150-mm dishes of either control HEK293 cells or HEK293 cells expressing MUSA1-V5 were lysed in a buffer containing 0.4% NP-40, 120 mM NaCl, 50 mM HEPES, pH 7.5, 2 mM 1,10-orthophenathroline, protease inhibitor cocktail and phosphatase inhibitor cocktail. Then, 60 µl of anti-V5 agarose resins was added, and samples were incubated for 4 h. Resins with the E3 complex bound were washed extensively, and recombinant E1 (20 nM), E2 (cdc34; 500 nM), ubiquitin (0.5 mg/ml) and ATP (5 mM) were added. After incubation at 37 °C for 5 h, reaction mixtures were separated by SDS-PAGE. The levels of ubiquitinated protein were determined by immunoblotting with FK2 antibody to ubiquitin (1:1,000 dilution; Enzo Life Sciences).

Histology, fluorescence microscopy and electron microscopy. Cryosections of transfected tibialis anterior muscles were examined by fluorescence microscope. Cryosections of tibialis anterior were stained for hematoxylin and eosin and for SDH. Cross-sectional area was measured for tibialis anterior as described[17,32] and compared with the area of surrounding untransfected myofibers (control). For morphometric studies, coimmunostaining was performed using rabbit antibody to laminin (1:500 dilution; Dako) together with mouse monoclonal antibody to pan–myosin heavy chain (undiluted supernatant of cultures of hybridoma cell clone A4-1025, DSHB) to visualize basal lamina and muscle fibers, respectively. Phosphorylated Smad1/5/8 was visualized using rabbit antibody to phosphorylated Smad1/5/8 (1:80 dilution; Cell Signaling Technology) together with mouse IgG2a antibody to dystrophin-1 (1:200 dilution; Novocastra) and DAPI, which allowed us to determine the subsarcolemmal position of myonuclei. Coimmunostaining for capillaries and muscle fibers was performed using antibody to CD31 (1:80 dilution; Pharmingen) and antibody to laminin (Dako). After washes in PBS, muscle sections were incubated for 45 min at room temperature with secondary antibodies, including Alexa Fluor 488 or Alexa Fluor 546 goat anti-rabbit IgG (Fab_2) and Alexa Fluor 647 or Alexa Fluor 488 goat anti-mouse IgG2a (all at a 1:400 dilution; Molecular Probes, Life Technologies), before being thoroughly washed with PBS, stained with DAPI and mounted with Fluoromount (Southern Biotech). Fiber typing was performed by immunofluorescence using combinations of the following monoclonal antibodies: BA-D5 that recognizes the type 1 myosin heavy chain isoform and SC-71 that recognizes the type 2A myosin heavy chain isoform. To detect primary antibodies, the following secondary antibodies were used: DyLight405-labeled goat anti-mouse IgG 2b subclass-specific (115-475-207) to specifically detect BA-D5 and DyLight488-labeled goat anti-mouse IgG1 subclass-specific (115-485-205) to specifically detect SC71. Secondary antibodies were purchased from Jackson ImmunoResearch. Images were captured using a CCD camera (ORCA ER, Hamamatsu Photonics) attached to a motorized fluorescence microscope (Zeiss AxioImager.Z1), and morphometric analyses were performed using the software Adobe Photoshop CS4 (Adobe) and MetaMorph 7.5 (Molecular Devices). Fiber diameter was calculated as the caliper width perpendicular to the longest chord of each myofiber. Total myofiber number was calculated from the entire muscle section using an assembled mosaic image (20× magnification). For electron microscopy, we used conventional fixation-embedding procedures based on glutaraldehyde-osmium fixation and Epon embedding.

Muscle physiology. *In vivo* determination of the force and contraction kinetics of gastrocnemius muscle was carried out as described previously[17,32,33]. Briefly, mice were anesthetized with a mixture of Xylor and Zoletil, and a small incision was made from the knee to the hip, exposing the sciatic nerve. Teflon-coated 7 multistranded steel wires (AS 632, Cooner Sales) were implanted before the branching of the sciatic nerve, with sutures on either side of the sciatic nerve. To avoid recruitment of the ankle dorsal flexors, the common peroneal nerve was cut. Torque production of the stimulated plantar flexors was measured using a muscle lever system (Model 305C, Aurora Scientific).

Ex vivo force measurements on soleus muscles were performed by dissecting this muscle from tendon to tendon under a stereomicroscope and subsequently mounting it between a force transducer (KG Scientific Instruments) and a micromanipulator-controlled shaft in a small chamber in which oxygenated Krebs solution was continuously circulated and the temperature was maintained at 25 °C. Stimulation conditions were optimized, and the length of the muscle was increased until force development during tetanus was maximal.

The function of tibialis anterior muscles was evaluated by measuring *in vivo* muscle contraction in response to nerve stimulation, as previously described[34]. Mice were anesthetized using intraperitoneal injection of

doi:10.1038/ng.2772

pentobarbital sodium at 50 mg/kg. The knee and paw were fixed in place, and the distal tendon of the muscle was attached to the lever arm of a servomotor system (305B, Dual-Mode Lever, Aurora Scientific) using a silk ligature. Data were analyzed using the PowerLab system (4SP, ADInstruments) and software (Chart 4, ADInstruments). The sciatic nerve was stimulated using supramaximal square-wave pulses of 0.1 ms in duration. Capacity for force generation was evaluated by measuring the absolute maximal force that was generated during isometric contractions in response to electrical stimulation (frequency of 75–150 Hz; train of stimulation of 500 ms). Maximal isometric force was determined at L_0 (length at which maximal tension was obtained during the tetanus). Force was normalized by muscle mass as an estimate of specific force. After force measurements, mice were sacrificed by cervical dislocation, and muscles were dissected, weighed and frozen in liquid nitrogen or in isopentane precooled in liquid nitrogen. Samples were stored at −80 °C for histological analyses.

Single-fiber preparation and mechanics. Bundles of fibers were dissected from the superficial layers of the gastrocnemius muscle and skinned as previously described[33]. In each fiber segment, isometric tension (Po) was measured during maximal activations at 20 °C, pCa = 4.8, under the conditions described in previous studies[32,33]. pCa is defined as $-\log_{10}$ of the calcium concentration.

Drug treatments. Wild-type CD1 mice were injected intraperitoneally with LDN-193189 hydrochloride by Axon Medchem at 3 mg/kg every 12 h for 9 d.

Statistical analysis and general experimental design. Sample size was calculated using size power analysis methods for a priori determination, based on the standard deviation and effect size previously obtained using the experimental methods employed in the study. For mouse studies, we estimated sample size from the expected number of knockout mice and littermate controls, which was based on mendelian ratios. We calculated the minimal sample size for each group to be at least four mice. Considering a likely drop-off effect of 10%, we set sample size for each group to five mice. To reduce the standard deviation, we minimized physiological variation by using homogenous mice of the same sex and same age. Exclusion criteria for mice were pre-established. In case of death, cannibalism or sickness, a mouse was excluded from analysis. Tissue samples were excluded in cases such as those with cryoartifacts, histological artifacts or failed RNA extraction. We included mice from different breeding cages by random allocation to the different experimental groups. Mouse experiments were not performed with blinding; however, when applicable, experimenters were blinded to the nature of the samples by using number codes until final data analysis was performed. Statistical tests were used as described in the figure legends and were applied upon verification of the test assumptions (for example, normality). Generally, data were analyzed by two-tailed Student's *t* test. For all graphs, data are represented as means ± s.e.m. For the measurement variables used to compare knockout mice and controls or innervated mice and denervated ones, the variance was similar between the groups.

26. Bardeesy, N. *et al.* Smad4 is dispensable for normal pancreas development yet critical in progression and tumor biology of pancreas cancer. *Genes Dev.* **20**, 3130–3146 (2006).
27. Bothe, G.W., Haspel, J.A., Smith, C.L., Wiener, H.H. & Burden, S.J. Selective expression of Cre recombinase in skeletal muscle fibers. *Genesis* **26**, 165–166 (2000).
28. McPherron, A.C., Lawler, A.M. & Lee, S.J. Regulation of skeletal muscle mass in mice by a new TGF-β superfamily member. *Nature* **387**, 83–90 (1997).
29. Akiyama, S. *et al.* Constitutively active BMP type I receptors transduce BMP-2 signals without the ligand in C2C12 myoblasts. *Exp. Cell Res.* **235**, 362–369 (1997).
30. Raffaello, A. *et al.* JunB transcription factor maintains skeletal muscle mass and promotes hypertrophy. *J. Cell Biol.* **191**, 101–113 (2010).
31. Carlson, M.E., Hsu, M. & Conboy, I.M. Imbalance between pSmad3 and Notch induces CDK inhibitors in old muscle stem cells. *Nature* **454**, 528–532 (2008).
32. Blaauw, B. *et al.* Akt activation prevents the force drop induced by eccentric contractions in dystrophin-deficient skeletal muscle. *Hum. Mol. Genet.* **17**, 3686–3696 (2008).
33. Blaauw, B. *et al.* Inducible activation of Akt increases skeletal muscle mass and force without satellite cell activation. *FASEB J.* **23**, 3896–3905 (2009).
34. Mouisel, E., Vignaud, A., Hourde, C., Butler-Browne, G. & Ferry, A. Muscle weakness and atrophy are associated with decreased regenerative capacity and changes in mTOR signaling in skeletal muscles of venerable (18–24-month-old) dystrophic *mdx* mice. *Muscle Nerve* **41**, 809–818 (2010).